



**HAL**  
open science

# Estimation of displacements from two frames obtained from stereo

Zhengyou Zhang, Olivier Faugeras

► **To cite this version:**

Zhengyou Zhang, Olivier Faugeras. Estimation of displacements from two frames obtained from stereo.  
[Research Report] RR-1440, INRIA. 1991. inria-00075120

**HAL Id: inria-00075120**

**<https://inria.hal.science/inria-00075120>**

Submitted on 24 May 2006

**HAL** is a multi-disciplinary open access archive for the deposit and dissemination of scientific research documents, whether they are published or not. The documents may come from teaching and research institutions in France or abroad, or from public or private research centers.

L'archive ouverte pluridisciplinaire **HAL**, est destinée au dépôt et à la diffusion de documents scientifiques de niveau recherche, publiés ou non, émanant des établissements d'enseignement et de recherche français ou étrangers, des laboratoires publics ou privés.

# INRIA

UNITÉ DE RECHERCHE  
INRIA-SOPHIA ANTIPOLIS

Institut National  
de Recherche  
en Informatique  
et en Automatique

Domaine de Voluceau  
Rocquencourt  
B.P.105  
78153 Le Chesnay Cedex  
France  
Tél.: (1) 39 63 55 11

## Rapports de Recherche

N° 1440

*Programme 4*  
*Robotique, Image et Vision*

### ESTIMATION OF DISPLACEMENTS FROM TWO 3D FRAMES OBTAINED FROM STEREO

Zhengyou ZHANG  
Olivier D. FAUGERAS

Juin 1991



\* R R - 1 4 4 0 \*

# **Estimation of Displacements from Two 3D Frames Obtained from Stereo\***

## **Estimation des déplacements à partir de deux scènes 3D reconstruites par un système stéréoscopique**

**Zhengyou Zhang    Olivier D. Faugeras**

INRIA Sophia-Antipolis

2004 route des Lucioles

06565 Valbonne Cedex, France

zzhang@mirsa.inria.fr    faugeras@mirsa.inria.fr

---

\*This work was supported in part by Esprit project P940.

## Abstract

We present a method for estimating 3D displacements from two stereo frames. It is based upon the hypothesize-and-verify paradigm which is used to match 3D line segments between the two frames. In order to reduce the complexity of the method, we make the assumption that objects are rigid. We formulate a set of complete rigidity constraints for 3D line segments and integrate the uncertainty of measurements in this formulation. The hypothesize and verify stages of the method use an Extended Kalman Filter to produce estimates of the displacements and of their uncertainty. In the experimental sections, the algorithm is shown to work on indoor and natural scenes. Furthermore it is easily extended, as also shown, to the case where several mobile objects are present. The method is quite robust, fast, and has been thoroughly tested on hundreds of real stereo frames.

**Keywords:** Motion from stereo, 3D matching, rigidity constraints, uncertainty, hypothesize-and-verify, multiple object motions, extended Kalman filtering, robot vision.

## Résumé

Nous présentons une méthode pour estimer des déplacements 3D à partir de deux triplets stéréoscopiques acquis de deux points de vues différentes. Elle est fondée sur le paradigme de génération et vérification d'hypothèses et est utilisée pour mettre en correspondance des segments de droite 3D entre les deux vues. Nous faisons l'hypothèse que des objets sont rigides afin de réduire la complexité de cette méthode. Nous formulons un ensemble complet de contraintes de rigidité pour les segments de droite 3D et l'incertitude de mesure est intégrée dans cette formulation. Un filtre de Kalman étendu est utilisé pendant les étapes de génération et vérification d'hypothèses pour estimer les déplacements et leur incertitude. Dans les sections expérimentales, nous montrons que l'algorithme a de bonnes performances dans des scènes naturelles aussi bien que dans des scènes intérieures. De plus, cet algorithme est facile à étendre pour résoudre le problème des mouvements d'objets multiples, comme il est détaillé dans ce rapport. Cette méthode a été testée avec quelques centaines de vrais triplets stéréoscopiques, ce qui montre qu'elle est très robuste et rapide.

**Mots clés:** Mouvement à partir de la stéréo, Appariement 3D, Contraintes de rigidité, Incertitude, Technique de génération et vérification d'hypothèses, Mouvements d'objets multiples, Filtre de Kalman étendu, Vision pour la robotique.

# Contents

<b>1</b>	<b>Introduction</b>	<b>3</b>
<b>2</b>	<b>Outline of the Matching Algorithm</b>	<b>5</b>
<b>3</b>	<b>Rigidity Constraints</b>	<b>5</b>
3.1	3D Rigid Displacement . . . . .	5
3.2	Rigidity Constraints . . . . .	8
<b>4</b>	<b>Representation of 3D Line Segments</b>	<b>9</b>
4.1	Motivation . . . . .	9
4.2	Our Representation . . . . .	10
4.2.1	Representing the orientation by its Euler angles $\phi$ and $\theta$ . . . . .	10
4.2.2	Modeling the midpoint of a 3D line segment . . . . .	11
<b>5</b>	<b>Error Measurements in the Constraints</b>	<b>12</b>
5.1	Norm Constraint . . . . .	13
5.2	Dot-Product Constraint . . . . .	14
5.3	Triple-Product Constraint . . . . .	14
<b>6</b>	<b>The Displacement Estimation Algorithm</b>	<b>15</b>
6.1	Generating Hypotheses . . . . .	15
6.2	Verifying Hypotheses . . . . .	16
6.2.1	Estimating the Initial Rigid Displacement . . . . .	16
6.2.2	Propagating Hypotheses . . . . .	16
6.2.3	Complexity . . . . .	17
6.2.4	Choosing the Best Hypothesis . . . . .	17
<b>7</b>	<b>Estimating 3D Displacement via an Extended Kalman Filter</b>	<b>17</b>
<b>8</b>	<b>Matching Noisy Line Segments</b>	<b>19</b>
8.1	Transformation of a 3D line segment . . . . .	19
8.2	Criterion of matching . . . . .	20
<b>9</b>	<b>Experimental Results</b>	<b>21</b>
9.1	Indoor Scene . . . . .	21
9.2	Rock Scene . . . . .	26
<b>10</b>	<b>Application to the Estimation of Multiple Object Displacements</b>	<b>27</b>
<b>11</b>	<b>Conclusion</b>	<b>34</b>
	<b>Appendix: Proof of Proposition 3</b>	<b>36</b>

## List of Figures

1	Diagram of the displacement analysis algorithm based on the hypothesize-and-verify paradigm . . . . .	6
2	Line segments undergoing a rigid displacement . . . . .	7
3	Definition of angles used in rigidity constraints . . . . .	9
4	Images of the first camera: the left one is at $t_1$ and the right one is at $t_2$ . . . .	21
5	Different views of stereo frame 1 (uniform scale) . . . . .	22
6	Different views of stereo frame 2 (uniform scale) . . . . .	23
7	Superposition of the two stereo frames: segments of Frame 1 are represented in dashed lines and those of Frame 2 in solid lines . . . . .	24
8	Superposition of the matched segments after applying the computed displacement to the segments of Frame 1: segments of Frame 1 are represented in dashed lines and those of Frame 2 in solid lines . . . . .	24
9	Superposition of the transformed segments of Frame 1 (in dashed lines) and those of Frame 2 (in solid lines) (non-uniform scale) . . . . .	25
10	Two images of a rock scene taken by the first camera . . . . .	27
11	Different views of stereo frame 1 (uniform scale) . . . . .	28
12	Different views of stereo frame 2 (uniform scale) . . . . .	29
13	Superposition of the transformed segments of Frame 1 (in dashed lines) and those of Frame 2 (in solid lines) (non-uniform scale) . . . . .	30
14	Images of the first camera of the trinocular stereo rig: the left one is in the first position and the right one is in the second position . . . . .	32
15	The front and top views of the reconstructed 3D frame in the first position . .	32
16	The front and top views of the reconstructed 3D frame in the second position .	33
17	Superposition of the two original frames . . . . .	33
18	Superposition of the segments of Frame 1 after applying the estimated egomotion and those of Frame 2 . . . . .	34
19	Superposition of the remaining segments of both frames after those matched through the egomotion estimation procedure have been eliminated . . . . .	35
20	Result of applying the estimated displacement of the box . . . . .	35
21	Congruency of two tetrahedra . . . . .	36
22	Reflection of two tetrahedra . . . . .	37
23	Completeness of the rigidity constraints: non-coplanar case . . . . .	37
24	Completeness of the rigidity constraints: coplanar case . . . . .	39

# 1 Introduction

Motion analysis is a very important research field in Robot Vision, and is essential for the interpretation of 3D dynamic scenes. Its applications include mobile robot navigation, scene segmentation, construction of a world model, dynamic surveillance and object tracking. Most previous research efforts have been on the motion analysis of a sequence of monocular images [1,2,3]. With the development of stereovision systems and range finders [4,5,6,7,8,9], the computation of motion from 3D data becomes a more attractive technique. Our research focuses on motion analysis from 3D frames which are obtained at different instants by a stereo system, when the mobile robot navigates in an unknown environment possibly containing some moving rigid objects. The features reconstructed by our stereo are 3D oriented line segments. The orientation is obtained from the image intensity contrast.

The problem of determining the three-dimensional structure and motion of objects from image data has been extensively studied by computer scientists for more than one decade. Table 1 summarizes the current approaches to motion analysis. They are first distinguished from each other according to whether they use either the changes of feature positions or those of gray levels between adjacent frames. The first approach is usually called *feature tracking* and the second, *optical flow*. In each case, one can consider the number of frames used: short sequence analysis (2 or 3 frames) or long sequence analysis (more than 4). One can further classify the current approaches according to the dimension of the available data. If we have only one image at each instant, we have only 2D data and the problem is called monocular sequence analysis. If we have two or three images at each instant, we can reconstruct 3D data using stereo and the problem is called binocular or trinocular sequence analysis. We can thus roughly divide existing methods into eight categories.

**Table 1:** Summary of Approaches to Motion Analysis

<i>changes</i>	<i>sequence</i>	<i>dimension</i>
<b>features</b>	<b>short (2 or 3)</b>	<b>2D</b>
<b>gray levels</b>	<b>long (<math>\geq 4</math>)</b>	<b>3D</b>

We do not intend to review here all previous work. The reader is referred to [10,11,12,13,14,15,16,17,18,19] for the work related to the optical flow approach, to [20,21,22,23,24,25,26,27,28,29,30,31] for the work related to the motion estimation from 2D feature correspondences over two or three frames, and to [32,33,34,35,36,37,38] for the work related to (2D or 3D) feature tracking approaches using a large number of frames. Those references are by no means exhaustive. The work reported in this paper falls into the category of motion analysis using 3D data from stereo over two frames.

The problem is usually tackled in two steps. The first step is to establish feature correspondences between two frames. The correspondence (matching) problem is recognized as a very difficult one. The rigidity assumption provides a powerful constraint to simplify the analysis, and is used in almost all matching algorithms. Pollard *et al.* [39] describe a matching strategy combining the local feature focus method proposed in [40,41] and the constrained tree-search technique using rigidity constraints proposed in [42]. Chen and Huang [43] propose an approach to match two sets of 3D points, which exploits also the rigidity constraints. Due to the completeness of the defined constraints for 3D points, that approach avoids extensive

comparisons of interrelationships and model tests like in the general tree-search approaches. The same authors presented in [44] an algorithm for matching 3D line segments. Using the point-matching algorithm described in [43], the directions of line segments can be matched. Several potential matchings may exist. For each potential matching, a rotation can be computed. In the second stage, a Hough-like procedure is used to prune those potential matchings and to compute a 3D translation which brings the (rotated) line segments into correspondences. Kim and Aggarwal [45] use a relaxation method to register two 3D frames from stereo. The constraints used are the distance and angle between a line and its neighbor. Once the feature correspondences are established, the second step is to estimate the 3D motion between the two frames. Many methods exist in the literature including analytic or numeric, linear or nonlinear, batch or recursive ones [46,47,48,49,50]. Due to the uncertainty in the measurements, these methods minimize some criteria (usually least-squares).

Under some restricted conditions, motion can be computed without registration between two frames. In [51] for example, 3D points are used, and the same set of points is assumed to be observed and to undergo the same motion between successive views. These assumptions are of course not realistic. Features may be visible in one view and not in another view due to, for example, occlusion, appearance or disappearance. Multiple moving objects may also exist in the scene.

It is worth noticing that motion analysis shares many common points with another important research field in Computer Vision - Object recognition and localization. Grimson and Lozano-Perez proposed in [42,52] a tree pruning approach using rigidity constraints to recognize 2D objects from 2D data or 3D objects from 3D data. For example, they used distance and angular constraints to match measured 3D points with model faces. To ensure the global consistency, model test is required. Their approach suffers from exponential combinatorics in case of spurious data and occluded objects. Bolle and Cooper reported in [53] an approach to 3D object recognition and positioning within a Bayesian estimation framework. Objects are represented by patches of primitive quadrics (planar, cylindrical, and spherical patches). Uncertainties of geometric primitives are described by probability density functions and 3D object position is estimated by maximizing a posteriori probability. Horaud and Bolles presented in [41] a technique to match 3D objects in range data using multiple primitives (straight lines, circular arcs and cylinders). The technique is the extension of the local-feature-focus approach proposed by Bolles and Cain in [40] to solve 2D object recognition problem. Another technique called generalized Hough transform or pose clustering [54,55] consists in finding directly a global transformation to bring into alignment the model and the observed object. The scheme of the algorithm presented in this paper is similar to those reported in [48,56] in the sense that all methods fall into the "hypothesize-and-verify" paradigm. Faugeras and Hébert proposed in [48] a method to match points and planar patches from range data with a list of planar patches in a stored model. Ayache and Faugeras described in [56] a method to match 2D line segments from polygonal approximation of an image to 2D objects in a model base represented also by 2D line segments. A similar approach is proposed by Lowe in [57,58] to recognize 3D object from 2D images. Lowe made use of perceptual organization to form structures in the image that are likely viewpoint invariant. Evidential reasoning was used to establish the initial feature correspondences. He iteratively updated the viewpoint estimation by adding more feature correspondences.

This paper deals with the analysis of motion or rather of displacement from two stereo views. In [59,60], we reported our preliminary work on this problem. This paper includes new developments, gives a more complete description of our approach and provides new results.



Since rigidity may be the most important constraint in two view motion analysis, we first provide a thorough description of it. We show that the rigidity constraints we formulate are complete for 3D line segments. The rigidity constraints are reformulated to take into account explicitly the uncertainty in measurements. We then develop an approach based on the *hypothesize-and-verify* paradigm for registering two stereo frames and computing the 3D displacement between them. The rigidity constraints formulated before are heavily used to generate hypotheses of primitive correspondences between two frames. We propose a new representation for 3D line segments in order to characterize the uncertainty caused by stereo. Using this representation, 3D displacement can be incrementally estimated via an extended Kalman filter and matching can be done efficiently. Finally, we provide two experimental examples and the application of this algorithm to multiple object motions.

## 2 Outline of the Matching Algorithm

The matching problem has been recognized as a very difficult problem. Given two sets of primitives observed in two views, the task of matching is to establish a correspondence between them. By a correspondence, we mean that the two paired primitives are the different observations (instances) of a single primitive undergoing motion. The matching problem has an exponential complexity in general. For example, if we structure the matching as a search in the interpretation tree [42], one should examine the consistency of  $(n + 1)^m$  interpretations, where  $n$  and  $m$  are the numbers of primitives in the two views. Recognizing this, we need some constraints to heuristically guide the search without exploring most of the nodes while making sure a good interpretation is found at the end.

The rigidity assumption about the environment and objects is used in most matching algorithms. Our approach uses that rigidity constraint to guide a hypothesize-and-verify method. The hypothesize-and-verify paradigm is one of the most popular paradigm to deal with the matching problem [40,42,41,48,56,39].

Our idea is simple. We use the rigidity constraints to generate some hypothetical primitive correspondences between two successive frames. We compute an initial estimate of the displacement for each hypothesis. We then evaluate the validity of these hypothetical displacements. Due to the rigidity constraints (see below), the number of hypothetical displacements is usually very small, and computational efficiency is achieved. We exploit the rigidity constraint locally in the hypothesis generation phase and globally in the hypothesis verification phase, as shown later. Figure 1 illustrates diagrammatically the principle of our hypothesize-and-verify method.

## 3 Rigidity Constraints

### 3.1 3D Rigid Displacement

It is well known that any 3D rigid displacement can be *uniquely* decomposed into a rotation around the origin of the coordinate system followed by a translation. Let  $P$  and  $P'$  be the position vectors of the same 3D point before and after displacement, the following relation holds:

$$P' = \mathbf{R}P + \mathbf{t}, \tag{1}$$

where  $\mathbf{R}$  is called the **Rotation Matrix** and  $\mathbf{t}$  is called the **translation vector** of the rigid displacement.  $(\mathbf{R}, \mathbf{t})$  must satisfy the following requirements.

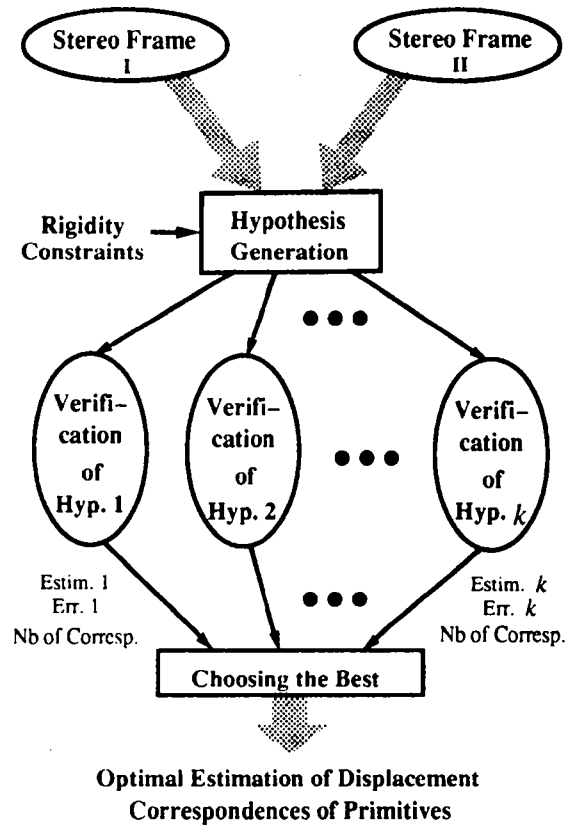


**Fig. 1:** Diagram of the displacement analysis algorithm based on the hypothesize-and-verify paradigm

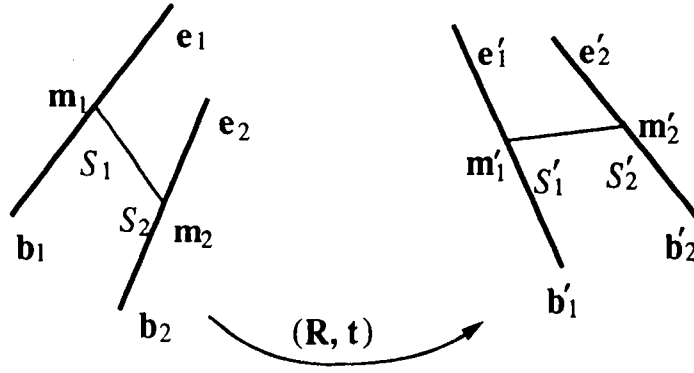


Fig. 2: Line segments undergoing a rigid displacement

**Definition 1**  $(\mathbf{R}, \mathbf{t})$  represents a rigid displacement if and only if the following requirements

- $\mathbf{R}$  is a  $3 \times 3$  orthogonal matrix and its determinant equals  $+1$ ,
- $\mathbf{t}$  is a real 3-dimensional vector,

are satisfied. ◇

Proposition 1 gives some interesting properties of the rotation matrix  $\mathbf{R}$  (the proof is omitted).

**Proposition 1** The Rotation Matrix  $\mathbf{R}$  has the following properties:

1.  $\mathbf{R}\mathbf{R}^T = \mathbf{R}^T\mathbf{R} = \mathbf{I}_3$ , and  $\mathbf{R}^{-1} = \mathbf{R}^T$ .
2.  $\|\mathbf{R}\mathbf{u}\| = \|\mathbf{u}\|$ ,
3.  $\mathbf{R}\mathbf{u} \cdot \mathbf{R}\mathbf{v} = \mathbf{u} \cdot \mathbf{v}$ ,
4.  $\mathbf{R}\mathbf{u} \wedge \mathbf{R}\mathbf{v} = \mathbf{R}(\mathbf{u} \wedge \mathbf{v})$ ,

where  $\mathbf{u}$  and  $\mathbf{v}$  are two arbitrary 3-dimensional vectors,  $^T$  denotes the transpose of a matrix,  $^{-1}$  denotes the inverse of a matrix,  $\|\cdot\|$  denotes the norm of a vector,  $\cdot$  denotes the inner product of two vectors, and  $\wedge$  denotes the cross product of two vectors. □

Consider now two line segments undergoing a rigid displacement (see Figure 2). The two segments are denoted by  $S_1$  and  $S_2$  before displacement and by  $S'_1$  and  $S'_2$  after displacement. We use the following notations: the unit direction vector of  $S$  is denoted by  $\mathbf{u}$  and the end-points are denoted by  $\mathbf{b}$  and  $\mathbf{e}$  (Remark: segments are oriented). If the rigid displacement is represented by  $(\mathbf{R}, \mathbf{t})$ , we have the following equations:

$$\mathbf{u}'_i = \mathbf{R}\mathbf{u}_i, \quad \mathbf{m}'_i = \mathbf{R}\mathbf{m}_i + \mathbf{t}, \quad \mathbf{b}'_i = \mathbf{R}\mathbf{b}_i + \mathbf{t}, \quad \mathbf{e}'_i = \mathbf{R}\mathbf{e}_i + \mathbf{t}, \quad \text{for } i = 1, 2. \quad (2)$$

### 3.2 Rigidity Constraints

Under rigid displacement, the geometry of a rigid object remains constant. In other words, the geometry of the object does not change during displacement. We want to derive specific constraints reflecting this invariance. The following requirements should be satisfied:

- The constraints should be independent of the coordinate systems. The relation between the coordinate systems is just what we want to compute.
- The constraints should be as complete as possible, to guarantee the global consistency of the final interpretation.
- The constraints should be as simple as possible, to allow efficient computation.

The following proposition gives necessary conditions.

**Proposition 2** *If two segments  $S_1$  and  $S_2$  in the first frame are matched to two segments  $S'_1$  and  $S'_2$  in the second frame, under the assumption of rigid displacement, the following constraints, called **Rigidity Constraints**, must be satisfied:*

#### 1. Length Constraints

$$l'_1 = l_1 \quad \text{and} \quad l'_2 = l_2; \quad (3)$$

#### 2. Distance Constraint

$$\|\mathbf{v}_{12}\| = \|\mathbf{v}'_{12}\|; \quad (4)$$

#### 3. Angular Constraints

$$(i) \quad \mathbf{u}_1 \cdot \mathbf{u}_2 = \mathbf{u}'_1 \cdot \mathbf{u}'_2; \quad (5)$$

$$(ii) \quad \mathbf{u}_1 \cdot \hat{\mathbf{v}}_{12} = \mathbf{u}'_1 \cdot \hat{\mathbf{v}}'_{12}; \quad (6)$$

$$(iii) \quad \mathbf{u}_2 \cdot \hat{\mathbf{v}}_{12} = \mathbf{u}'_2 \cdot \hat{\mathbf{v}}'_{12}; \quad (7)$$

#### 4. Triple Product Constraint

$$\langle \mathbf{u}_1, \mathbf{u}_2, \hat{\mathbf{v}}_{12} \rangle = \langle \mathbf{u}'_1, \mathbf{u}'_2, \hat{\mathbf{v}}'_{12} \rangle. \quad (8)$$

In the above,  $\langle \mathbf{u}_1, \mathbf{u}_2, \mathbf{u}_3 \rangle$  denotes the triple product (i.e.,  $\mathbf{u}_1 \cdot (\mathbf{u}_2 \wedge \mathbf{u}_3)$ ),  $\mathbf{v}_{12}$  is the vector joining the midpoints (i.e.,  $\mathbf{v}_{12} = \mathbf{m}_2 - \mathbf{m}_1$ ) and  $\hat{\mathbf{v}}_{12}$  is a unit length vector parallel to  $\mathbf{v}_{12}$  (i.e.,  $\hat{\mathbf{v}}_{12} = \mathbf{v}_{12}/\|\mathbf{v}_{12}\|$ ).  $\square$

The above proposition can be easily verified using Equations 2 and the properties of rigid displacement described in Proposition 1. See the appendix for the proof.

In the rigidity constraints, three angles are involved ( $\theta$ ,  $\theta_1$  and  $\theta_2$  in Figure 3). In this figure, the segment  $//S_2$  is parallel to segment  $S_2$  and shares a common endpoint with  $S_1$ . Instead of angles, we use the cosine of angles. Equation 5 implies the conservation of the angle between  $S_1$  and  $S_2$  (i.e., the angle  $\theta$  between  $S_1$  and  $//S_2$ ). Equation 6 implies the conservation of the angle  $\theta_1$  between  $S_1$  and the segment  $\mathbf{v}_{12}$  joining the midpoints. Equation 7 implies the conservation of the angle  $\theta_2$  between  $S_2$  and  $\mathbf{v}_{12}$ .

The reverse of Proposition 2 is proved in [61]. Therefore we have:

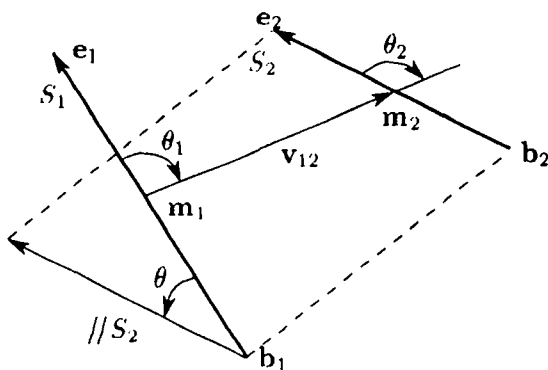


Fig. 3: Definition of angles used in rigidity constraints

**Proposition 3** *The rigidity constraints given in Proposition 2 are complete for 3D line segments, in the sense that they are necessary and sufficient to guarantee the congruency of two sets of line segments.*  $\square$

The following proposition follows.

**Proposition 4** *The displacement computed from two pairings of non-collinear segments satisfying the rigidity constraints in Proposition 2 is rigid and unique.*  $\square$

Since two pairings of non-collinear segments satisfying the rigidity constraints implies the congruency of two tetrahedra (or quadrilaterals) from Proposition 3, a unique rigid displacement can be computed. See [61] for the proof.

## 4 Representation of 3D Line Segments

Before proceeding further, we briefly describe in this section how to represent 3D line segments. The 3D line segments we have (from stereo or other sensors) are inherently uncertain and usually do not have the same error distribution in different directions. It has been recognized in the Computer Vision and Robotics community [62,63] that uncertainty should be explicitly represented and manipulated. Two representations of uncertainty in 3D reconstruction from stereo are available. Blostein and Huang [64] assumed that the pixel errors were uniformly distributed and the 3D points reconstructed by stereo triangulation were also assumed to be uniformly distributed in the corresponding volume. Instead, Matthies and Shafer [65] modeled the stereo triangulation errors as three-dimensional Gaussian distributions and claimed that it gave good results in stereo navigation when the distance to points is not extreme (see also [66]). The later modelization makes possible efficient and tractable computation. For the same reason, we also model measurement errors as Gaussian. However, we should remember that this assumption can only be justified for small random errors and not for systematic errors.

### 4.1 Motivation

A line is usually represented by its endpoints  $M_1$  and  $M_2$ , which require 6 parameters, and their covariance matrices  $A_1$  and  $A_2$ .  $A_1$  and  $A_2$  are estimated from stereo triangulation from

point correspondences [67]. Equivalently, a line segment can be represented by its direction vector  $\mathbf{v}$  and its midpoint  $M$ , and their covariance matrices. But we cannot use directly these parameters in most cases. The endpoints or the midpoint of a segment are not reliable. The reason for this is that the way the uncertainty of the endpoints of a three-dimensional segment is computed takes only into account the uncertainty in pixel location due to edge detection and the uncertainty in the calibration of the stereo rig [66]. But it does not take into account the uncertainty due to the variations in segmentation of the polygonal approximation process. There are two main sources for those variations. The first one is purely algorithmic: because of noise in the image and because we sometimes approximate curved contours with straight line segments, the polygonal approximation may vary from frame to frame inducing a variation in the segments endpoints yet unaccounted for. The second is physical: because of partial occlusion in the scene, a segment can be considerably shortened or lengthened and this also has to be taken into account in the modeling of uncertainty.

Thus, instead of the line segment, the infinite line supporting the segment is usually used, as in [45]. In an earlier version of our algorithm for displacement analysis from two stereo views [50,59,60], a line segment was treated in a mixed way. The infinite supporting line was used in estimating the displacement, and the line segment was used for matching. There has been a lot of representations proposed for a line in the literature [63,68]. The main problem is that **the uncertainty on the line parameterization does not reflect that of the segment which the line supports** (see [61] for more details). A segment with big uncertainty may result in small uncertainty in the line parametrization. In the next subsection, we describe a representation for 3D line segments taking into account the variations in segmentation.

## 4.2 Our Representation

Due to the deficiencies of the previous representations for a line or a line segment, we use a five parameter representation for a line segment: two for the orientation, and three for the position of a point on the segment. This is a trade-off between line and segment. If we add another parameter for the length, the line segment is fully specified. Special care is given to the representation of uncertainty.

### 4.2.1 Representing the orientation by its Euler angles $\phi$ and $\theta$

Consider the spherical coordinates. Let  $\mathbf{u} = [u_x, u_y, u_z]^T$  be a unit vector of orientation, we have:

$$\begin{cases} u_x = \cos \phi \sin \theta \\ u_y = \sin \phi \sin \theta \\ u_z = \cos \theta \end{cases} \quad (9)$$

with  $0 \leq \phi < 2\pi$ .  $0 \leq \theta \leq \pi$ .

From  $\mathbf{u}$ , we can compute  $\phi$ ,  $\theta$ :

$$\begin{aligned} \phi &= \begin{cases} \arccos \frac{u_x}{\sqrt{1-u_z^2}} & \text{if } u_y \geq 0 \\ 2\pi - \arccos \frac{u_x}{\sqrt{1-u_z^2}} & \text{otherwise} \end{cases} \\ \theta &= \arccos u_z. \end{aligned} \quad (10)$$

If we denote  $[\phi, \theta]^T$  by  $\Psi$ , then the mapping between  $\Psi$  and  $\mathbf{u}$  is 1-to-1, except when  $\theta = 0$ . When  $\theta = 0$ ,  $\phi$  is not defined. Fortunately, the component corresponding to  $\phi$  in the

covariance matrix computed below will be very large in this case, as shown in [61]. This means that the measurement  $\phi$  has no information. Another problem with this representation is the discontinuity of  $\phi$  when a segment varies nearly parallel to the plane  $y = 0$ . In that case, the angle  $\phi$  may jump from the interval  $[0, \pi/2)$  to the interval  $(3\pi/2, 2\pi)$ , or *vice versa*. This discontinuity must be dealt with in matching and integration.

In the following, we assume that the direction vector  $\mathbf{v} = [x, y, z]^T$  and its covariance matrix  $\Lambda_{\mathbf{v}}$  of a given segment are known. We want to compute  $\phi$  and its covariance matrix  $\Lambda_{\phi}$  from  $\mathbf{v}$  and  $\Lambda_{\mathbf{v}}$ . From Equation 10,  $\phi$  and  $\theta$  are simply given by:

$$\begin{aligned}\phi &= \begin{cases} \arccos \frac{x}{\sqrt{x^2+y^2}} & \text{if } y \geq 0 \\ 2\pi - \arccos \frac{x}{\sqrt{x^2+y^2}} & \text{otherwise} \end{cases} \\ \theta &= \arccos \frac{z}{\sqrt{x^2+y^2+z^2}}.\end{aligned}\quad (11)$$

Since the relation between  $\Psi$  and  $\mathbf{v}$  is not linear, we use the first order approximation to compute the covariance matrix  $\Lambda_{\Psi}$  from  $\Lambda_{\mathbf{v}}$ . That is

$$\Lambda_{\Psi} = \frac{\partial \Psi}{\partial \mathbf{v}} \Lambda_{\mathbf{v}} \frac{\partial \Psi^T}{\partial \mathbf{v}}, \quad (12)$$

where the Jacobian matrix  $\frac{\partial \Psi}{\partial \mathbf{v}} = \begin{bmatrix} \frac{\partial \phi}{\partial x} & \frac{\partial \phi}{\partial y} & \frac{\partial \phi}{\partial z} \\ \frac{\partial \theta}{\partial x} & \frac{\partial \theta}{\partial y} & \frac{\partial \theta}{\partial z} \end{bmatrix}$ .

#### 4.2.2 Modeling the midpoint of a 3D line segment

We choose the midpoint as the point on the segment, but a special treatment of the covariance is introduced to characterize the uncertainty in the location of a segment.

The midpoint  $M$  and its covariance matrix  $\Lambda_M$  can be computed from the endpoints of the segment by:

$$M = (M_1 + M_2)/2 \text{ and } \Lambda_M = (\Lambda_1 + \Lambda_2)/4.$$

As described earlier, the measurement of endpoints is not reliable. The position of a segment may vary along its direction in different views. So, we model the midpoint  $\mathbf{m}$  as follows:

$$\mathbf{m} = (M_1 + M_2)/2 + n\mathbf{u}, \quad (13)$$

where  $\mathbf{u}$  is the unit direction vector of the segment and  $n$  is a random scalar independent of  $M_1$  and  $M_2$ . Equation 13 says in fact that the midpoint of a segment is only partially credible: it may vary randomly along the line supporting it in successive views. As explained before, the main reason of this modelization is that the uncertainty measures of  $M_1$  and  $M_2$  given by the stereo system modelize only the uncertainties due to stereo triangulation, but not those due to, for example, different segmentations. Remark that this modelization is in accordance with the definition of a line. If a point  $\mathbf{p}_0$  on a line and its orientation  $\mathbf{u}$  are given, the line  $L$  may be defined as a set of points in 3D space parametrized by a real variable  $t$ :

$$L = \{\mathbf{p} \mid \mathbf{p} = \mathbf{p}_0 + t\mathbf{u}, -\infty < t < \infty\}. \quad (14)$$

The random variable  $n$  in Equation 13 is modeled as Gaussian, zero-mean, with deviation  $\sigma_n$ , a positive scalar. If a segment is reliable,  $\sigma_n$  may be chosen to be a small number; if not,

it may be chosen to be a big number. In our implementation,  $\sigma_n$  is related to the length  $l$  of the segment, *i.e.*,  $\sigma_n = \kappa l$ , where  $\kappa$  is some constant independent of the segment. That is to say, the longer a segment is, the bigger the deviation  $\sigma_n$  is. That is reasonable since a long segment is much likely to be broken into smaller segments in other views due to, for example, occlusion. In our experiments,  $\kappa = 0.2$ .

In order to compute the covariance of  $\mathbf{m}$ , we should first compute  $\mathbf{u}$  and  $\Lambda_{\mathbf{u}}$ . The unit direction vector  $\mathbf{u}$  and its covariance  $\Lambda_{\mathbf{u}}$  can be computed from the non-normalized direction vector  $\mathbf{v}$  and its covariance matrix  $\Lambda_{\mathbf{v}}$ . Indeed, we have

$$\mathbf{u} = \frac{\mathbf{v}}{\|\mathbf{v}\|}, \quad \Lambda_{\mathbf{u}} = \frac{\partial \mathbf{u}}{\partial \mathbf{v}} \Lambda_{\mathbf{v}} \frac{\partial \mathbf{u}}{\partial \mathbf{v}}^T, \quad (15)$$

where  $\frac{\partial \mathbf{u}}{\partial \mathbf{v}}$  is a  $3 \times 3$  matrix ( $\frac{\partial \mathbf{u}}{\partial \mathbf{v}} = \frac{\mathbf{I}_3}{\|\mathbf{v}\|} - \frac{\mathbf{v}\mathbf{v}^T}{\|\mathbf{v}\|^3}$ ). Note that the covariance matrix  $\Lambda_{\mathbf{u}}$  is singular (the determinant is zero). This is of course because the three components of  $\mathbf{u}$  are not independent.

At this point, the covariance of  $\mathbf{m}$  can be computed. Equation 13 can be rewritten down as

$$\mathbf{m} = M + n\mathbf{u}. \quad (16)$$

Since  $n$  and  $\mathbf{u}$  are independent of each other, we have

$$\mathbf{E}[n\mathbf{u}] = \mathbf{E}[n]\mathbf{E}[\mathbf{u}] = \mathbf{0}, \quad (17)$$

$$\Lambda_{n\mathbf{u}} = \mathbf{E}[(n\mathbf{u})(n\mathbf{u})^T] = \mathbf{E}[n^2]\mathbf{E}[\mathbf{u}\mathbf{u}^T] = \sigma_n^2(\Lambda_{\mathbf{u}} + \bar{\mathbf{u}}\bar{\mathbf{u}}^T), \quad (18)$$

where  $\bar{\mathbf{u}}$  denotes  $\mathbf{E}[\mathbf{u}]$ , and

$$\mathbf{E}[\mathbf{m}] = \mathbf{E}[M], \quad (19)$$

$$\Lambda_{\mathbf{m}} = \mathbf{E}[(\mathbf{m} - \mathbf{E}[\mathbf{m}])(\mathbf{m} - \mathbf{E}[\mathbf{m}])^T] = \Lambda_M + \Lambda_{n\mathbf{u}}. \quad (20)$$

If we add another parameter  $l$  to denote the length of the segment, we can then represent exactly a line segment. This ends our modelization of a line segment. See [69,61] for more details.

## 5 Error Measurements in the Constraints

In Section 3, we have proposed a number of rigidity constraints for 3D line segments, and shown that they were complete (necessary and sufficient conditions for the existence of a rigid displacement). We have also shown that we can compute a unique rigid displacement from two pairings of segments satisfying the rigid constraints. However, all derivations were based on the noise-free assumption. The data we have are always corrupted with noise, due to uncertainties in polygonal approximation, stereo calibration and reconstruction. The equalities in Proposition 2 are not true anymore. In this section, we reformalize the rigidity constraints by explicitly taking into account the uncertainty of measurements. The idea is to compute *dynamically* a threshold for each constraint from the uncertainty in 3D data as modeled in the last section. The reader is referred to [42,39,44,70] for other formalisms of rigidity constraints in the literature. Unlike our approach, all those approaches use some predefined error ranges in the measurements. However, the errors of measurements given by a stereo system have



different distributions in different positions. One cannot handle such phenomena with some prefixed values.

Examining Proposition 2, we find that the rigidity constraints take three forms:

$$(i) \text{ Norm Constraint} \quad \|\mathbf{v}\| = \|\mathbf{v}'\| \quad (21)$$

$$(ii) \text{ Dot-Product Constraint} \quad \mathbf{u} \cdot \mathbf{v} = \mathbf{u}' \cdot \mathbf{v}' \quad (22)$$

$$(iii) \text{ Triple-Product Constraint} \quad \langle \mathbf{u}_1, \mathbf{u}_2, \mathbf{u}_3 \rangle = \langle \mathbf{u}'_1, \mathbf{u}'_2, \mathbf{u}'_3 \rangle \quad (23)$$

## 5.1 Norm Constraint

The norm constraint says that the difference between the norms of two vectors should be zero. For convenience, we use the squared norm of a vector instead of its norm. Taking into account the uncertainty of measurements, we can formalize the constraint as follows:

$$|\|\mathbf{v}\|^2 - \|\mathbf{v}'\|^2| < \varepsilon_n, \quad (24)$$

where  $\varepsilon_n$  is the threshold to be determined on the norm constraint.

Replacing  $\|\mathbf{v}\|^2 - \|\mathbf{v}'\|^2$  by  $d_n$ , then we have

$$d_n = \mathbf{v} \cdot \mathbf{v} - \mathbf{v}' \cdot \mathbf{v}' = \mathbf{v}^T \mathbf{v} - \mathbf{v}'^T \mathbf{v}'. \quad (25)$$

Given the covariance matrix  $\Lambda_{\mathbf{v}}$  of  $\mathbf{v}$  and the covariance matrix  $\Lambda_{\mathbf{v}'}$  of  $\mathbf{v}'$ , we now compute the variance  $\Lambda_{d_n}$  of  $d_n$ . Under the first order approximation, we have

$$\Lambda_{d_n} = J_{\mathbf{v}}^{d_n} \Lambda_{\mathbf{v}} J_{\mathbf{v}}^{d_n T} + J_{\mathbf{v}'}^{d_n} \Lambda_{\mathbf{v}'} J_{\mathbf{v}'}^{d_n T}, \quad (26)$$

where  $J_{\mathbf{v}}^{d_n}$  is the Jacobian matrix of  $d_n$  with respect to  $\mathbf{v}$  and  $J_{\mathbf{v}'}^{d_n}$ , the one with respect to  $\mathbf{v}'$ . Here we assume that  $\mathbf{v}$  and  $\mathbf{v}'$  are two independent Gaussian random variables.

The Jacobian  $J_{\mathbf{v}}^{d_n}$  is given by

$$J_{\mathbf{v}}^{d_n} = \frac{\partial d_n}{\partial \mathbf{v}} = \frac{\partial}{\partial \mathbf{v}} (\mathbf{v}^T \mathbf{v} - \mathbf{v}'^T \mathbf{v}') = 2\mathbf{v}^T. \quad (27)$$

Similarly, we have  $J_{\mathbf{v}'}^{d_n} = -2\mathbf{v}'^T$ . Now Equation 26 can be rewritten down as

$$\Lambda_{d_n} = 4(\mathbf{v}^T \Lambda_{\mathbf{v}} \mathbf{v} + \mathbf{v}'^T \Lambda_{\mathbf{v}'} \mathbf{v}'). \quad (28)$$

So, the norm constraint (Equation 21) is finally expressed in the real case as

$$\frac{d_n^2}{\Lambda_{d_n}} < \kappa_n, \quad (29)$$

where  $d_n$  is computed by Equation 25,  $\Lambda_{d_n}$  by Equation 28, and  $\kappa_n$  is a coefficient.

In fact,  $\frac{d_n^2}{\Lambda_{d_n}}$  can be considered up to the first order approximation that we have used, as a random variable following a  $\chi^2$  distribution with 1 degree of freedom. Looking at the  $\chi^2$  table, we can choose an appropriate value for  $\kappa_n$ . This gives us the probability that  $d_n^2$  falls into the interval  $[0, \kappa_n \Lambda_{d_n}]$ . For example, we can take  $\kappa_n = 3.84$  for a probability of 95% when we consider the lengths of segments, and  $\kappa_n = 1.32$  for a probability of 75% when we consider the distance between the midpoints of the two segments. That is, we impose a stricter constraint on the distance between midpoints than on the lengths of segments.

## 5.2 Dot-Product Constraint

The dot-product constraint says that the difference between the cosines of angles between two vectors should be zero. Suppose we are given two vectors  $\mathbf{u}$  and  $\mathbf{v}$ , and their covariance matrices  $\Lambda_{\mathbf{u}}$  and  $\Lambda_{\mathbf{v}}$ . Here,  $\mathbf{u}$  and  $\mathbf{v}$  are assumed unit vectors. Denote the difference between the cosines of angles as  $d_c$ , *i.e.*

$$d_c = \mathbf{u} \cdot \mathbf{v} - \mathbf{u}' \cdot \mathbf{v}' = \mathbf{u}^T \mathbf{v} - \mathbf{u}'^T \mathbf{v}'. \quad (30)$$

We now compute the variance  $\Lambda_{d_c}$  of  $d_c$ . Under the first order approximation, we have

$$\Lambda_{d_c} = J_{\mathbf{u}}^{d_c} \Lambda_{\mathbf{u}} J_{\mathbf{u}}^{d_c T} + J_{\mathbf{v}}^{d_c} \Lambda_{\mathbf{v}} J_{\mathbf{v}}^{d_c T} + J_{\mathbf{u}'}^{d_c} \Lambda_{\mathbf{u}'} J_{\mathbf{u}'}^{d_c T} + J_{\mathbf{v}'}^{d_c} \Lambda_{\mathbf{v}'} J_{\mathbf{v}'}^{d_c T}, \quad (31)$$

where  $J_{\mathbf{u}}^{d_c}$ ,  $J_{\mathbf{v}}^{d_c}$ ,  $J_{\mathbf{u}'}^{d_c}$  and  $J_{\mathbf{v}'}^{d_c}$  are the Jacobian matrices of  $d_c$  with respect to  $\mathbf{u}$ ,  $\mathbf{v}$ ,  $\mathbf{u}'$  and  $\mathbf{v}'$ , respectively. We assume that  $\mathbf{u}$ ,  $\mathbf{v}$ ,  $\mathbf{u}'$  and  $\mathbf{v}'$  are four independent Gaussian random variables.

The Jacobian  $J_{\mathbf{u}}^{d_c}$  is given by

$$J_{\mathbf{u}}^{d_c} = \frac{\partial d_c}{\partial \mathbf{u}} = \frac{\partial}{\partial \mathbf{u}} (\mathbf{u}^T \mathbf{v} - \mathbf{u}'^T \mathbf{v}') = \mathbf{v}^T. \quad (32)$$

Similarly, we have

$$J_{\mathbf{v}}^{d_c} = \mathbf{u}^T, \quad J_{\mathbf{u}'}^{d_c} = -\mathbf{v}'^T, \quad \text{and} \quad J_{\mathbf{v}'}^{d_c} = -\mathbf{u}'^T. \quad (33)$$

Equation 31 can be rewritten down as

$$\Lambda_{d_c} = \mathbf{v}^T \Lambda_{\mathbf{u}} \mathbf{v} + \mathbf{u}^T \Lambda_{\mathbf{v}} \mathbf{u} + \mathbf{v}'^T \Lambda_{\mathbf{u}'} \mathbf{v}' + \mathbf{u}'^T \Lambda_{\mathbf{v}'} \mathbf{u}'. \quad (34)$$

So, the dot-product constraint (Equation 22) is finally expressed in the real case as

$$\frac{d_c^2}{\Lambda_{d_c}} < \kappa_c, \quad (35)$$

where  $d_c$  is computed by Equation 30,  $\Lambda_{d_c}$  by Equation 34, and  $\kappa_c$  is a coefficient. We can choose  $\kappa_c = 1.32$  for a probability of 75%.

## 5.3 Triple-Product Constraint

The same manipulation can be done for the mix-product constraint. Given 6 unit vectors:  $\mathbf{u}_1$ ,  $\mathbf{u}_2$ ,  $\mathbf{u}_3$ ,  $\mathbf{u}'_1$ ,  $\mathbf{u}'_2$ ,  $\mathbf{u}'_3$  and their covariance matrices. Denote the difference between the two triple-products by  $d_t$ , *i.e.*

$$d_t = \langle \mathbf{u}_1, \mathbf{u}_2, \mathbf{u}_3 \rangle - \langle \mathbf{u}'_1, \mathbf{u}'_2, \mathbf{u}'_3 \rangle. \quad (36)$$

We can compute the covariance  $\Lambda_{d_t}$  of  $d_t$  under the first order approximation. The mix-product constraint (Equation 23) is then expressed in the real case as

$$\frac{d_t^2}{\Lambda_{d_t}} < \kappa_t, \quad (37)$$

where  $\kappa_t$  is a coefficient.

In our implementation, however, we do not compute the variance of the  $d_t$ , because the computation is relatively expensive. Instead, we give a predefined threshold  $\varepsilon_t$ . If  $|d_t| < \varepsilon_t$ , then the mix-product constraint is considered satisfied; otherwise, not satisfied.  $|d_t|$  reaches a maximum of 2 when  $\mathbf{u}_1$ ,  $\mathbf{u}_2$ ,  $\mathbf{u}_3$  are perpendicular to each other,  $\mathbf{u}'_1$ ,  $\mathbf{u}'_2$ ,  $\mathbf{u}'_3$  are perpendicular to each other, and they are not congruent (*i.e.*, reflection).  $|d_t|$  reaches a minimum of 0 when they are congruent. We have chosen  $\varepsilon_t = 0.5$  in our implementation to account for noise.

## 6 The Displacement Estimation Algorithm

In this section, we present an algorithm based on the hypothesis-and-verify paradigm to register two stereo frames and to estimate the displacement between them. We assume that the environment is static and that it is only the stereo rig that has moved.

### 6.1 Generating Hypotheses

At the first stage, the rigidity constraints are heavily used to generate hypotheses of matches between the two frames. Two pairings of segments form a plausible hypothesis if they satisfy the rigidity constraints described in the previous sections. If we explore all possible pairs, the complexity is  $O(m^2n^2)$ , where  $m$  is the number of segments in the first frame and  $n$  that in the second frame. The generation of hypotheses is implemented as follows. For a segment  $S_1$  in the first frame, we find a segment  $S'_1$  in the second frame such that its length is compatible with that of  $S_1$ . For the pairing  $(S_1, S'_1)$ , we then find the pairings  $(S_k, S'_k)$  such that the two pairings form a plausible hypothesis. When we are done, we go to the next segment  $S_2$  of the first frame.

Since at this stage we do not want to recover all matches between two frames, but to recover all potential displacements between them, we reduce the complexity of the hypothesis generation phase by using a number of heuristics:

**Sort the segments** Sort all segments in each frame in decreasing length order, so that we can easily find, by binary search, the segments in the second frame which are compatible in length with the segments in the first one.

**Control the depth** Rather than finding all possible pairings compatible with a given pairing, we stop if we have found a sufficient number of compatible pairings (5, for instance).

**Avoid redundant hypotheses** If a pairing has already been retained as a potential match in some earlier hypothesis, it is not considered further, because it does not give us new information about the displacement between two frames.

**Reduce the width** Consider segments of the first frame only in the central part of the frame, because segments on the sides are likely to have moved out of the field of view in the next frame.

**Reduce the number of segments** Choose only the longest segments in the first scene, for instance, the  $m/q$  longest ( $q = 2$  or  $3$ ). This reduces also the search width.

Other constraints can be integrated in the algorithm to speed up even more the generation process. In the indoor mobile robot navigation example, the robot and the objects usually move horizontally (in the ground plane). In our stereo coordinate system, the ground plane is parallel to the plane  $y = 0$ . Thus we can impose the constraint that if two segments can be matched to each other, they must have almost the same  $y$  coordinates. Another constraint we can use is on the change of the orientation of a segment [60]. In general, the rotation angle between two successive frames does not go beyond 60 degrees, so we can impose that the orientation difference of a pairing of segments to be matched must be less than 60 degrees.

## 6.2 Verifying Hypotheses

At the second stage of the algorithm, we propagate each hypothesis generated above to the whole frame and try to match more segments. We then choose the best hypotheses, best being defined later. This can be done in parallel for each hypothesis. The process is performed as follows.

### 6.2.1 Estimating the Initial Rigid Displacement

From Proposition 4, we know that a unique rigid displacement can be computed for each hypothesis. We compute an initial estimation of the rotation and translation via an Extended Kalman Filter (see Section 7). An initial guess of the state vector (representing the rigid displacement) is required as input to the filter. In our implementation, the state vector  $\mathbf{s}$  for the displacement is simply initialized to zero (*i.e.*  $\hat{\mathbf{s}}_0 = \mathbf{0}$ ) but with a big covariance matrix. The covariance matrix  $\Lambda_{\hat{\mathbf{s}}_0}$  is initialized as follows:  $\Lambda_{\hat{\mathbf{s}}_0}[i][i] = 2.0$  for  $i = 0, 1, 2$  (rotation components),  $\Lambda_{\hat{\mathbf{s}}_0}[i][i] = 1.0 \times 10^6$  for  $i = 3, 4, 5$  (translation components) and  $\Lambda_{\hat{\mathbf{s}}_0}[i][j] = 0$  for  $i \neq j$ . This is equivalent to saying that we assume a standard deviation of 114 degrees of rotation along each axis and a standard deviation of 1 meter of translation along each axis.

Because we use a first order approximation, if the initial estimate is not very good, the final estimate given by the filter may be different from the true value. In order to reduce the effect of nonlinearities, we can apply the Kalman filter iteratively. Usually, we obtain a good estimate after a few iterations (typically 3 or 4).

### 6.2.2 Propagating Hypotheses

We now have an initial estimate of the displacement for each hypothesis. We apply this estimate to the first frame and compare the transformed frame with the second one. If a transformed segment from the first frame is near enough to some segment in the second frame, then this pair is considered as matched (see Section 8 for the definition of near enough), and again, the Extended Kalman Filter is used to update the displacement estimate. After all segments have been processed, we obtain an estimate of the displacement, its uncertainty and also the correspondences between segments.

We said that we transformed all segments of the first frame once, using the initial estimate of displacement. This is the one-shot approach. The matching results will depend heavily upon this initial estimate. Since we may have a poor initial estimate, we may not get a satisfactory matching result. To overcome this problem, we transform only one non-matched segment of the first frame at a time. This is the many-shots approach. If we find a match for it, we update the displacement estimate and transform another non-matched segment of the first frame using the new updated estimation of the displacement (not the initial estimate any more). If we cannot find a match, we process another segment of the first frame. After all segments have been processed, we obtain an estimate of the displacement, its uncertainty, and also the correspondences between segments.

We have implemented the two approaches and found that the second one gives much better performances. Starting from two slightly different initial estimates, the first approach yields two different (not dramatically different, of course) results of matchings and displacement estimates, while the second converges to almost the same result.

In order to obtain a precise estimation and because of the nonlinearities, we iterate the above procedure twice.

### 6.2.3 Complexity

We note that the complexity of the algorithm in the worst case is  $O(mn)$  for each hypothesis. The speed of the algorithm depends essentially on the ability to access quickly to the segments of Frame 2 which are close to a transformed segment  $\hat{S}$ . We have used several approaches to achieve this. One approach is to use binary search to discard segments of Frame 2 which are not compatible in length with  $S$ . Another efficient method is to use **bucketing techniques**, which allow us to obtain a list of segments in the neighborhood of some segment. The preprocessing necessary to sort segments into buckets can be done very quickly (the complexity is linear in the number of segments).

### 6.2.4 Choosing the Best Hypothesis

We now discuss how to choose the best hypothesis using the error given by the Kalman filter. The criterion must be a function of the number of segments actually matched and of the error made in approximating the match by a rigid displacement. We use the following criterion:

$$C = \sum_{i=1}^p E_i + (N - p)E_{min} \quad (38)$$

where  $E_i$  is the error of the  $i$ -th match (the sum of the distances given by Equations 53 and 54, see Section 8), and  $N = \min(m, n)$  is the smallest number of segments in the two scenes,  $p$  is the number of segments matched and  $E_{min}$  is the error corresponding to the threshold determining when two segments are matched (which is equal to  $\kappa_{\Psi} + \kappa_{\mathbf{m}}$  given in Section 8). Then, the hypothesis with a minimal  $C$  is chosen as the best one. From Equation 38, we can see that the more matches we have, the smaller the error is. Note that if we simply define  $C$  as  $p$  (the number of segments matched) and choose the hypothesis with a maximal  $C$  as the best one, almost the same result is obtained.

## 7 Estimating 3D Displacement via an Extended Kalman Filter

Given a set of correspondences of 3D primitives (points, line segments and planar patches), many methods are reported in the literature to estimate 3D displacement [46,48,49,45,71,50]. A comparison of several of those methods has been carried out using 3D line segment correspondences (see [72]). This work reveals that the extended Kalman filter (EKF) should be preferred for its efficiency and accuracy. We assume that the reader is familiar with the ideas and equations of the Kalman filter [73,74], which have now become of standard use in Vision.

The standard Kalman filter is a powerful tool to deal with parameter estimation problems in a linear noisy system. However, it is not directly applicable to our problem, because of its nonlinearity. The EKF approach [73,75] is to apply the standard Kalman filter to *nonlinear* systems with additive Gaussian noise by continually updating a *linearization* around the previous state estimate, starting with an initial guess. Here we formulate the displacement estimation problem using the representation of 3D line segments described in Section 4 in order to apply the EKF. We first briefly describe our representation of rotations.

Many representations exist for 3D rotations, including Euler angles, quaternions and rotation axis [11,76]. We use the rotation axis representation. More precisely, a rotation can be defined as a three-dimensional vector  $\mathbf{r} = [a, b, c]^T$  whose direction is that of the axis of

rotation and whose magnitude is equal to the rotation angle. The relation between  $\mathbf{r}$  and the rotation matrix  $\mathbf{R}$  is given by the following formula, known as Rodrigues formula [77]

$$\mathbf{R} = \mathbf{I}_3 + \frac{\sin \theta}{\theta} \tilde{\mathbf{r}} + \frac{1 - \cos \theta}{\theta^2} \tilde{\mathbf{r}}^2 \quad (39)$$

where  $\theta$  is the norm of  $\mathbf{r}$  (i.e.,  $\theta = \|\mathbf{r}\|$ ),  $\mathbf{I}_3$  is the  $3 \times 3$  identity matrix and  $\tilde{\mathbf{r}}$  is the antisymmetric matrix defined as

$$\tilde{\mathbf{r}} = \begin{bmatrix} 0 & -c & b \\ c & 0 & -a \\ -b & a & 0 \end{bmatrix}.$$

This matrix represents the cross-product with vector  $\mathbf{r}$ , since  $\tilde{\mathbf{r}}\mathbf{x} = \mathbf{r} \wedge \mathbf{x}$  for all  $x$ . A 3D displacement is then represented by the 6-dimensional vector  $\mathbf{s} = [\mathbf{r}^T, \mathbf{t}^T]^T$ .

For reason of simplicity, we define two non-linear functions  $\mathbf{g}$  and  $\mathbf{h}$  to relate a unit vector  $\mathbf{u}$  and its Euler angles  $\Psi$  (see Equations 9 and 10), such that

$$\Psi = \mathbf{g}(\mathbf{u}) \quad \text{and} \quad \mathbf{u} = \mathbf{h}(\Psi). \quad (40)$$

If a segment  $S$  is characterized by  $(\Psi_1, \mathbf{m}_1)$  in Frame 1 and by  $(\Psi_2, \mathbf{m}_2)$  in Frame 2, and that the displacement between the two frames is  $\mathbf{s} = [\mathbf{r}^T, \mathbf{t}^T]^T$ , then we have the following equations

$$\Psi_2 = \mathbf{g}(\mathbf{R}\mathbf{h}(\Psi_1)), \quad (41)$$

$$\mathbf{m}_2 = \mathbf{R}\mathbf{m}_1 + \mathbf{t}. \quad (42)$$

The above equations simply say that the *transformed* segment of the first frame should have the same orientation and location as the segment observed in the second frame. If we define the measurement vector as

$$\mathbf{x} = [\Psi_1^T, \mathbf{m}_1^T, \Psi_2^T, \mathbf{m}_2^T]^T, \quad (43)$$

then we can write down the measurement equation from Equations 41 and 42 as

$$\mathbf{f}(\mathbf{x}, \mathbf{s}) = \begin{bmatrix} \mathbf{g}(\mathbf{R}\mathbf{h}(\Psi_1)) - \Psi_2 \\ \mathbf{R}\mathbf{m}_1 + \mathbf{t} - \mathbf{m}_2 \end{bmatrix} = \mathbf{0}. \quad (44)$$

This is a 5-dimensional vector equation. In the following, the first two components of  $\mathbf{f}(\mathbf{x}, \mathbf{s})$  are denoted by  $\mathbf{f}_1$  and the last three components by  $\mathbf{f}_2$ .

Equation 44 can be expanded into a Taylor series around the current displacement estimate  $\hat{\mathbf{s}}$  and the current observation  $\hat{\mathbf{x}}$ :

$$\mathbf{f}(\mathbf{x}, \mathbf{s}) = \mathbf{f}(\hat{\mathbf{x}}, \hat{\mathbf{s}}) + \frac{\partial \mathbf{f}(\hat{\mathbf{x}}, \hat{\mathbf{s}})}{\partial \mathbf{x}} (\mathbf{x} - \hat{\mathbf{x}}) + \frac{\partial \mathbf{f}(\hat{\mathbf{x}}, \hat{\mathbf{s}})}{\partial \mathbf{s}} (\mathbf{s} - \hat{\mathbf{s}}) + O((\mathbf{x} - \hat{\mathbf{x}})^2) + O((\mathbf{s} - \hat{\mathbf{s}})^2). \quad (45)$$

Ignoring the second order terms, we get a linearized measurement equation:

$$\mathbf{y} = \mathbf{M}\mathbf{s} + \mathbf{v}, \quad (46)$$

where  $\mathbf{y}$  is the new measurement vector,  $\mathbf{v}$  is the noise vector of the new measurement, and  $\mathbf{M}$  is the linearized transformation matrix. They are given by

$$\mathbf{M} = \frac{\partial \mathbf{f}(\hat{\mathbf{x}}, \hat{\mathbf{s}})}{\partial \mathbf{s}},$$

$$\begin{aligned}
\mathbf{y} &= -\mathbf{f}(\hat{\mathbf{x}}, \hat{\mathbf{s}}) + \frac{\partial \mathbf{f}(\hat{\mathbf{x}}, \hat{\mathbf{s}})}{\partial \mathbf{s}} \hat{\mathbf{s}}, \\
\mathbf{v} &= \frac{\partial \mathbf{f}(\hat{\mathbf{x}}, \hat{\mathbf{s}})}{\partial \mathbf{x}} (\mathbf{x} - \hat{\mathbf{x}}), \\
E[\mathbf{v}] &= \mathbf{0}, \\
E[\mathbf{v}\mathbf{v}^T] &= \frac{\partial \mathbf{f}(\hat{\mathbf{x}}, \hat{\mathbf{s}})}{\partial \mathbf{x}} \Lambda_{\hat{\mathbf{x}}} \frac{\partial \mathbf{f}(\hat{\mathbf{x}}, \hat{\mathbf{s}})}{\partial \mathbf{x}}^T.
\end{aligned}$$

The standard Kalman filter can then be applied to the above linearized system to update the displacement estimate  $\hat{\mathbf{s}}$ . The derivatives of  $\mathbf{f}(\mathbf{x}, \mathbf{s})$  with respect to  $\mathbf{s}$  and to  $\mathbf{x}$  are computed as follows:

$$\frac{\partial \mathbf{f}}{\partial \mathbf{s}} = \begin{bmatrix} \frac{\partial \mathbf{f}_1}{\partial \mathbf{r}} & \mathbf{0} \\ \frac{\partial \mathbf{f}_2}{\partial \mathbf{r}} & \mathbf{I}_3 \end{bmatrix}, \quad (47)$$

$$\frac{\partial \mathbf{f}}{\partial \mathbf{x}} = \begin{bmatrix} \frac{\partial \mathbf{f}_1}{\partial \Psi_1} & \mathbf{0} & -\mathbf{I}_2 & \mathbf{0} \\ \mathbf{0} & \mathbf{R} & \mathbf{0} & -\mathbf{I}_3 \end{bmatrix}, \quad (48)$$

where

$$\begin{aligned}
\frac{\partial \mathbf{f}_1}{\partial \mathbf{r}} &= \frac{\partial \mathbf{g}(\mathbf{u}'_1)}{\partial \mathbf{u}} \frac{\partial (\mathbf{R}\mathbf{u}_1)}{\partial \mathbf{r}}, \\
\frac{\partial \mathbf{f}_2}{\partial \mathbf{r}} &= \frac{\partial (\mathbf{R}\mathbf{m}_1)}{\partial \mathbf{r}}, \\
\frac{\partial \mathbf{f}_1}{\partial \Psi_1} &= \frac{\partial \mathbf{g}(\mathbf{u}'_1)}{\partial \mathbf{u}} \mathbf{R} \frac{\partial \mathbf{h}(\Psi_1)}{\partial \Psi},
\end{aligned}$$

with  $\mathbf{u}_1 = \mathbf{h}(\Psi_1)$  and  $\mathbf{u}'_1 = \mathbf{R}\mathbf{u}_1$ . The reader is referred to [61] for the computation of the derivatives  $\frac{\partial (\mathbf{R}\mathbf{u}_1)}{\partial \mathbf{r}}$ ,  $\frac{\partial (\mathbf{R}\mathbf{m}_1)}{\partial \mathbf{r}}$ ,  $\frac{\partial \mathbf{g}(\mathbf{u}'_1)}{\partial \mathbf{u}}$  and  $\frac{\partial \mathbf{h}(\Psi_1)}{\partial \Psi}$ .

Each time a new match becomes available, we can incrementally update the displacement estimate  $\mathbf{s}$  via EKF using the above formulation.

## 8 Matching Noisy Line Segments

Suppose now that we have an estimate of the displacement  $\mathbf{s} = [\mathbf{r}^T, \mathbf{t}^T]^T$  between the two frames with its covariance matrix  $\Lambda_{\mathbf{s}}$ . The question is: for a given segment  $S$  in Frame 1, which segment in Frame 2 can it be matched to? Our solution goes in two steps. The segment  $S$  is first transformed into  $\hat{S}$  by applying the given displacement estimate. It is then compared with segments in Frame 2.

### 8.1 Transformation of a 3D line segment

Let the parametrization of the segment  $S$  be  $(\Psi, \mathbf{m})$  and that of the transformed segment  $\hat{S}$  be  $(\hat{\Psi}, \hat{\mathbf{m}})$ . Clearly, we have

$$\hat{\Psi} = \mathbf{g}(\mathbf{R}\mathbf{h}(\Psi)), \quad (49)$$

$$\hat{\mathbf{m}} = \mathbf{R}\mathbf{m} + \mathbf{t}. \quad (50)$$

If the uncertainty measure of the segment  $S$  is given by  $(\Lambda_\Psi, \Lambda_{\mathbf{m}})$ , then we can compute the covariance matrix  $\Lambda_{\hat{\Psi}}$  of  $\hat{\Psi}$ , under the first order approximation, as

$$\Lambda_{\hat{\Psi}} = J_{\hat{\Psi}} \Lambda_\Psi J_{\hat{\Psi}}^T + J_s \Lambda_s J_s^T, \quad (51)$$

where the Jacobian matrices are given by

$$\begin{aligned} J_{\hat{\Psi}} &= \frac{\partial \mathbf{g}(\hat{\mathbf{u}})}{\partial \mathbf{u}} \mathbf{R} \frac{\partial \mathbf{h}(\Psi)}{\partial \Psi}, \\ J_s &= \begin{bmatrix} \frac{\partial \mathbf{g}(\hat{\mathbf{u}})}{\partial \mathbf{u}} \frac{\partial (\mathbf{R}\mathbf{u})}{\partial \mathbf{r}} & \mathbf{0}_3 \end{bmatrix} \end{aligned}$$

with  $\mathbf{u} = \mathbf{h}(\Psi)$ ,  $\hat{\mathbf{u}} = \mathbf{R}\mathbf{u}$  and  $\mathbf{0}_3$  is the  $3 \times 3$  null matrix.

Similarly, the covariance matrix  $\Lambda_{\hat{\mathbf{m}}}$  of the midpoint  $\hat{\mathbf{m}}$  is given by

$$\Lambda_{\hat{\mathbf{m}}} = \mathbf{R} \Lambda_{\mathbf{m}} \mathbf{R}^T + J_s^{\hat{\mathbf{m}}} \Lambda_s J_s^{\hat{\mathbf{m}T}}, \quad (52)$$

where the Jacobian matrix of  $\hat{\mathbf{m}}$  with respect to  $\mathbf{s}$  is

$$J_s^{\hat{\mathbf{m}}} = \begin{bmatrix} \frac{\partial (\mathbf{R}\mathbf{m})}{\partial \mathbf{r}} & \mathbf{I}_3 \end{bmatrix}.$$

The reader is referred to [61] for the computation of the derivatives.

## 8.2 Criterion of matching

Now we have a representation of the segment  $\hat{S}$  and a set of segments  $\{S_i | i = 1..n\}$  in Frame 2. We want to decide which segment  $S_i$  can be matched with  $\hat{S}$ .

Using the representation of 3D line segments described in Section 4, matching can be done very efficiently. It goes in two steps. Let the segment  $S_i$  be represented by  $(\Psi_i, \mathbf{m}_i)$  and its covariance matrices  $(\Lambda_{\Psi_i}, \Lambda_{\mathbf{m}_i})$ . We want to know whether  $S_i$  can be matched with  $\hat{S}$  or not. The first step is to examine the similarity in orientation. The Mahalanobis distance between the orientations is given by

$$d_\Psi = (\Psi - \Psi_i)^T (\Lambda_\Psi + \Lambda_{\Psi_i})^{-1} (\Psi - \Psi_i). \quad (53)$$

If  $d_\Psi$  is less than some threshold  $\kappa_\Psi$ , we then go to the second step: examine the distance between the midpoints of two segments. The Mahalanobis distance between the midpoints is given by

$$d_{\mathbf{m}} = (\mathbf{m} - \mathbf{m}_i)^T (\Lambda_{\mathbf{m}} + \Lambda_{\mathbf{m}_i})^{-1} (\mathbf{m} - \mathbf{m}_i). \quad (54)$$

If  $d_{\mathbf{m}}$  is still less than some threshold  $\kappa_{\mathbf{m}}$ , we then consider the two segments as matched.

Before computing the Mahalanobis distance between the  $\Psi$ 's (Equation 53), special care is required to cope with the discontinuity of  $\phi$  when a segment is nearly parallel to the plane  $y = 0$  (see Section 4). The treatment is very simple: if  $\phi < \pi/2$  and  $\phi_i > 3\pi/2$ , then set  $\phi_i = \phi_i - 2\pi$ ; else if  $\phi > 3\pi/2$  and  $\phi_i < \pi/2$ , then set  $\phi = \phi - 2\pi$ ; else do nothing. Note that adding a constant to a random variable does not affect its covariance matrix.

By choosing appropriately the threshold  $\kappa_\Psi$  and  $\kappa_{\mathbf{m}}$ , we can recover almost all possible matches. From the  $\chi^2$  distribution table, we take  $\kappa_\Psi = 6.0$  for a probability of 95% with 2 degrees of freedom, and  $\kappa_{\mathbf{m}} = 7.8$  for a probability of 95% with 3 degrees of freedom.



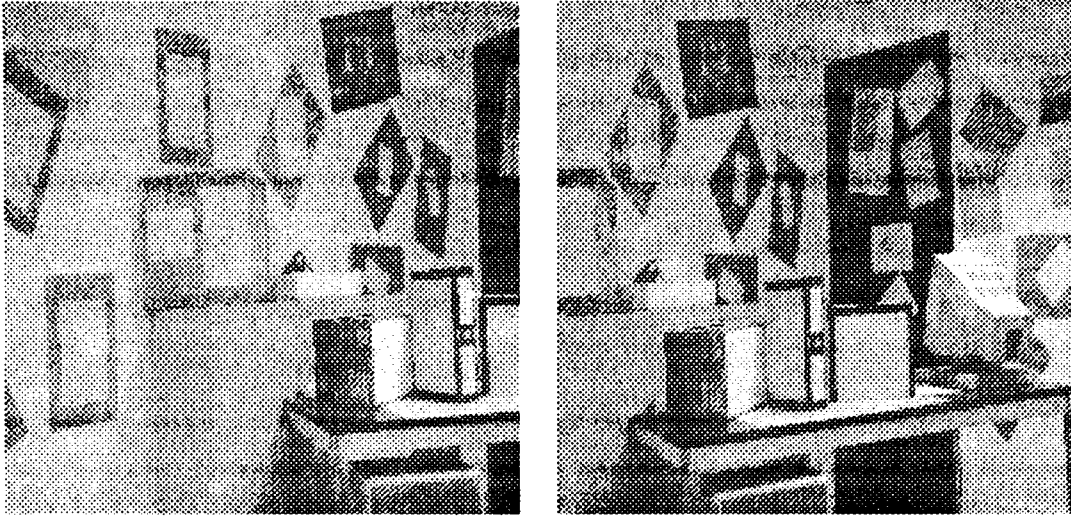


Fig. 4: Images of the first camera: the left one is at  $t_1$  and the right one is at  $t_2$

## 9 Experimental Results

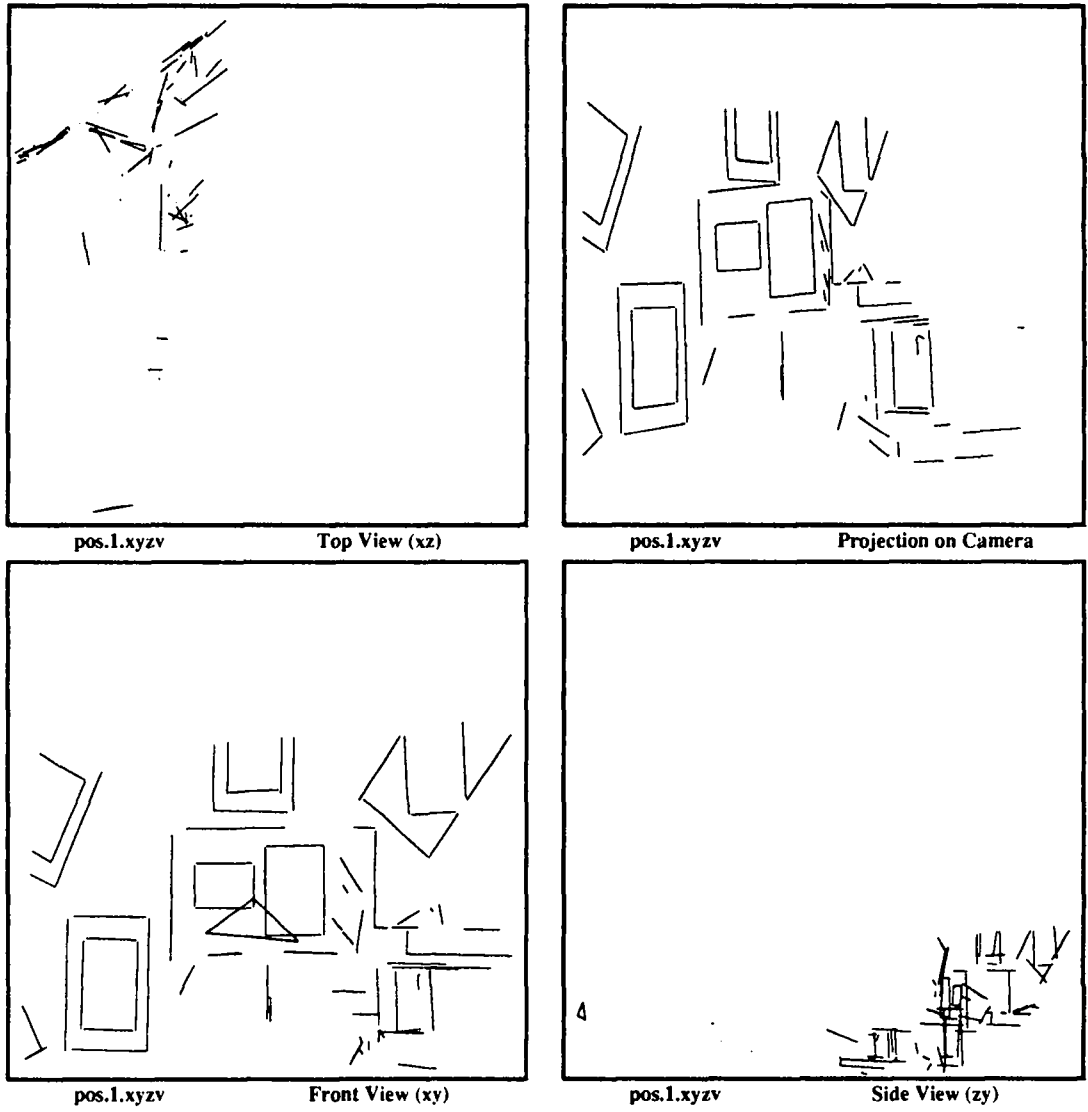
The algorithm presented in this paper has been tested for two years using real stereo data acquired by our trinocular stereo system. At least two hundred pairs of stereo frames (*i.e.*, 400 individual stereo frames) have been used. The algorithm has succeeded in correctly matching and computing the 3D displacement and matching two views in almost all cases. The few cases of failure are due to too little common intersection (less than 20%) between the two stereo frames.

The reader can find some experimental results in [60]. In this section, we provide two examples to demonstrate the matching process. In each figure shown, if there are four pictures, the upper left one is the top view (projection on the ground plane), the lower left one is the front view (projection on a plane in front of the stereo system and perpendicular to the ground plane), the lower right one is a side view (projection on the plane which is perpendicular to the previous two planes) and the upper right is the view from the first camera (perspective projection using the calibrated camera transformation matrix). If there are only two pictures in each figure, then the left one is the front view and the right one is the top view.

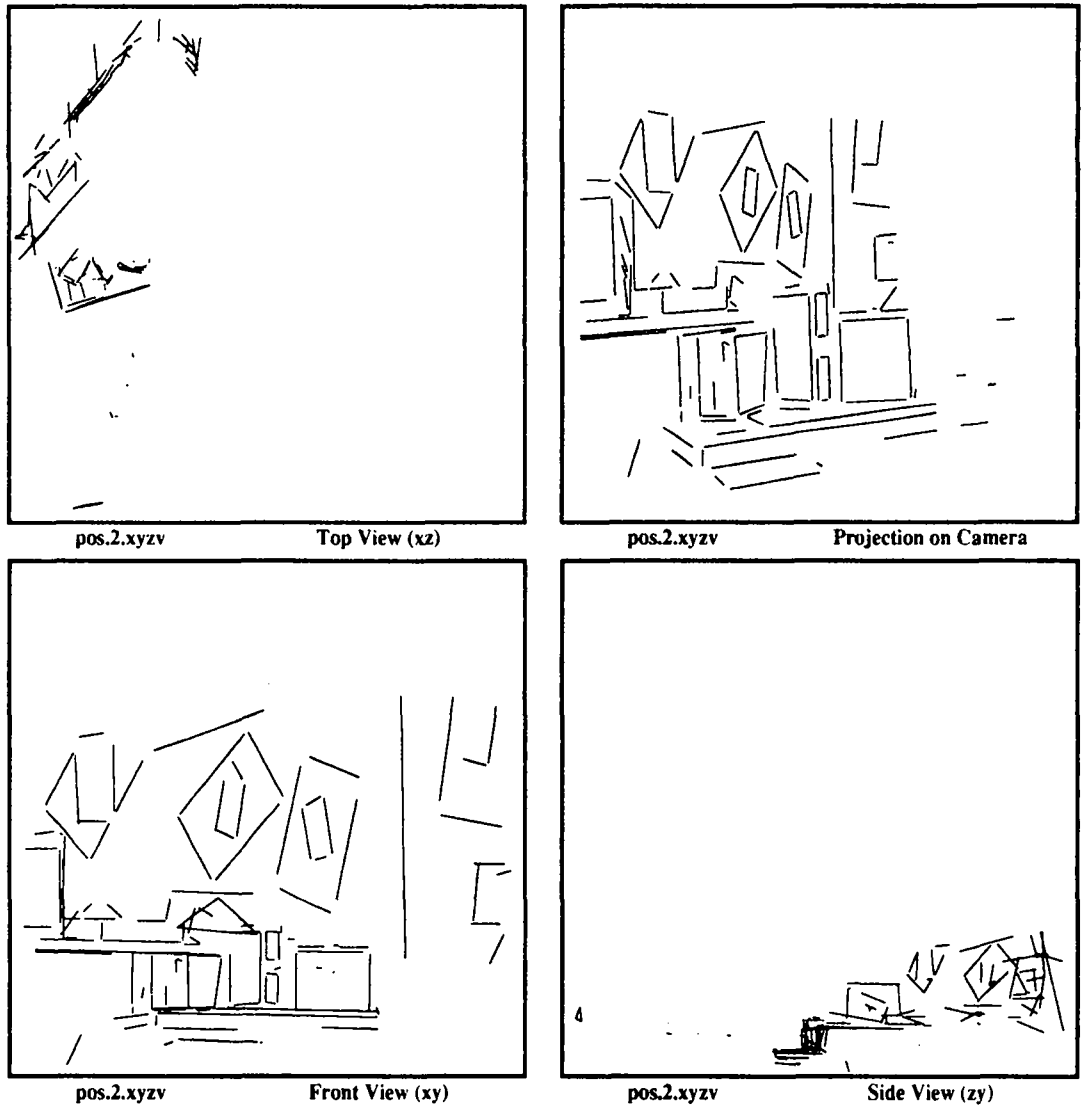
### 9.1 Indoor Scene

Figure 4 shows the images of an indoor scene taken by the first camera of the stereo rig at two instants. As can be observed, there is only a small common part between two successive frames. In fact, there is a big rotation between the two views. Comparing the two images in Figure 4, the boxes on the table have a displacement of about 200 pixels in the image plane (resolution: 512×512).

Figures 5 and 6 show the pair of stereo frames reconstructed by our trinocular stereo. The triangle in each picture represents the optical centers of the three cameras. We have 79 segments in the first frame and 121 segments in the second. There is a rotation of about 16.5 degrees between the two positions, which can be noticed by superposing the two frames (see



**Fig. 5:** Different views of stereo frame 1 (uniform scale)



**Fig. 6:** Different views of stereo frame 2 (uniform scale)

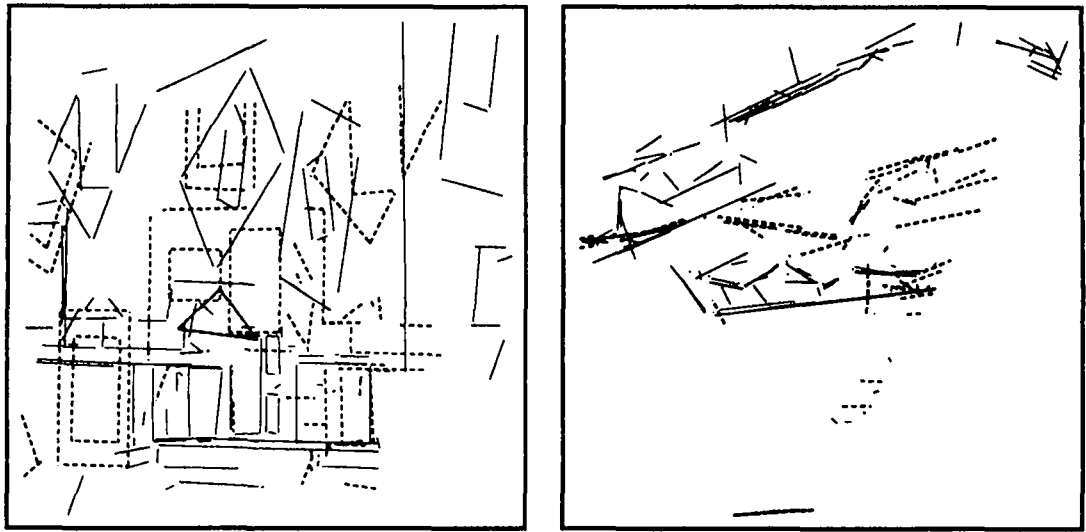


**Fig. 7:** Superposition of the two stereo frames: segments of Frame 1 are represented in dashed lines and those of Frame 2 in solid lines

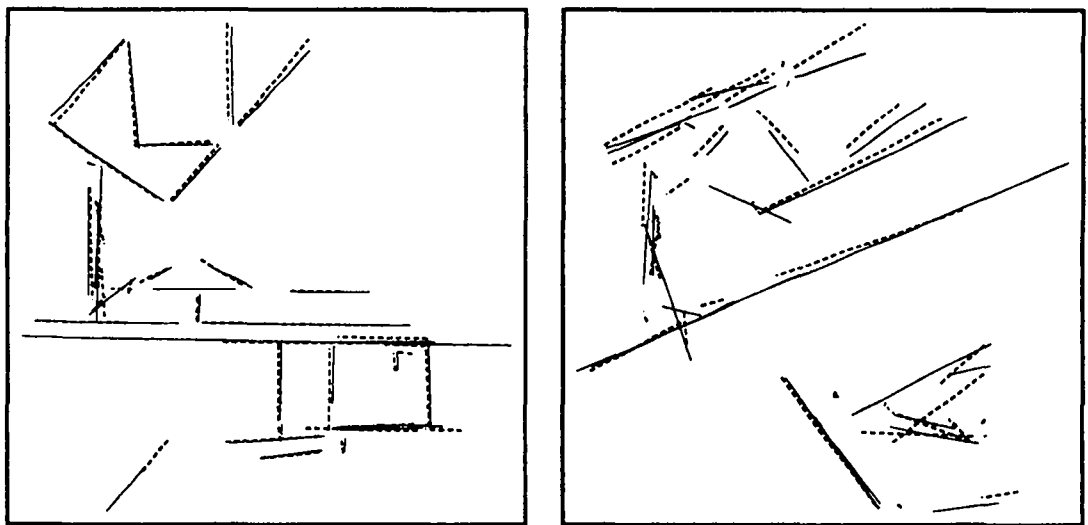


**Fig. 8:** Superposition of the matched segments after applying the computed displacement to the segments of Frame 1: segments of Frame 1 are represented in dashed lines and those of Frame 2 in solid lines

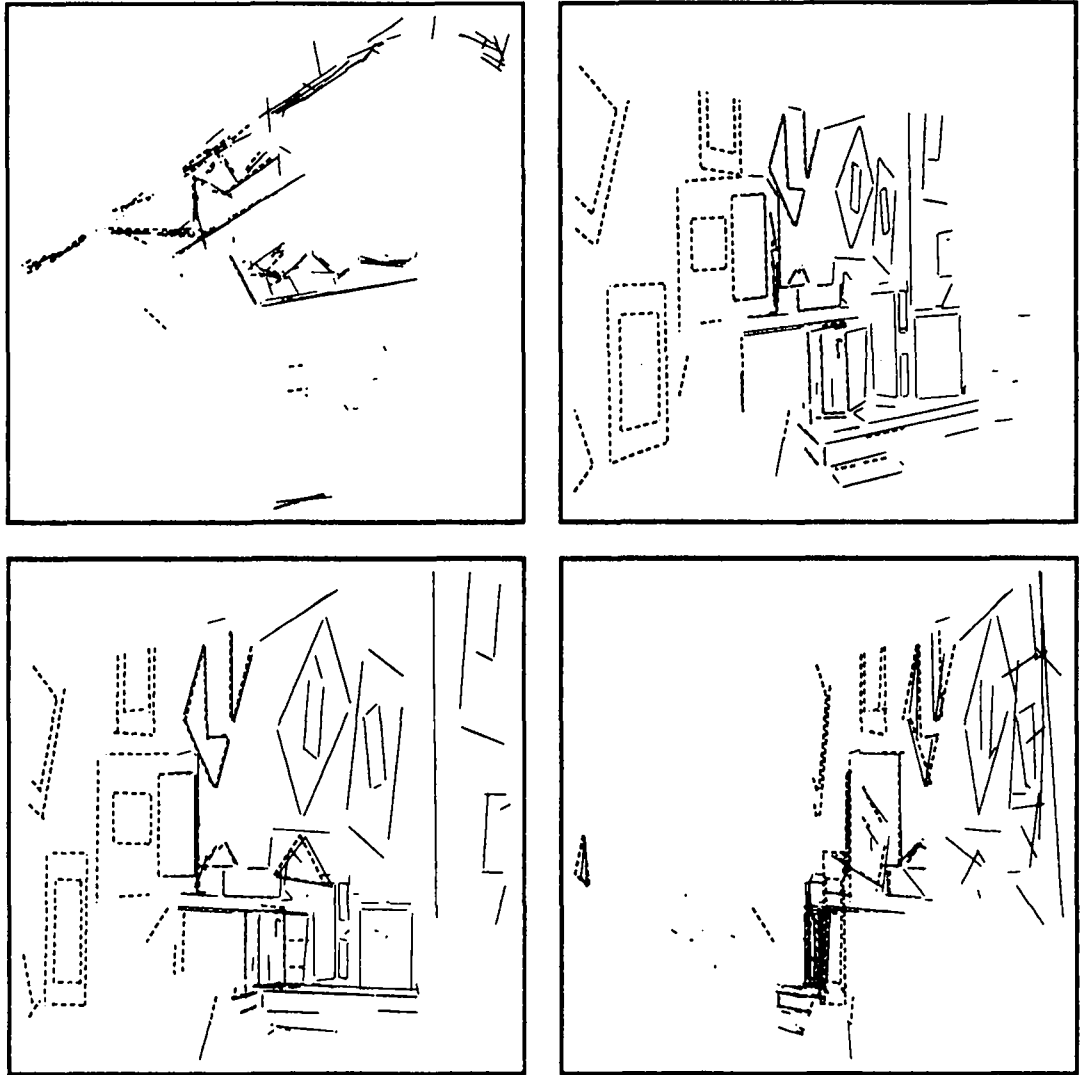


**Fig. 9:** Superposition of the transformed segments of Frame 1 (in dashed lines) and those of Frame 2 (in solid lines) (non-uniform scale)

Figure 7).

Applying the displacement estimation algorithm to these two frames, we obtain 5 hypotheses. All five hypotheses are propagated to the whole frame to match more segments and to update the displacement estimate. In the end, 4 hypotheses yield the correct estimate of the displacement. 37 matches are recovered. To determine how good this estimate is, we apply the computed estimate to the first frame and superimpose the transformed one on the second. Figure 8 shows such superposition of the matched segments and Figure 9 shows the superposition of the whole frames. The estimate of displacement is very good. We can observe the rotation between the two positions by the shift of the two triangles in Figure 9. We observe also that the common part is very small. The whole process takes about 50 seconds on a SUN 3 workstation.

Several remarks can be made at this point:

- Segments in the foreground (near the observer) are better superimposed than others. This is reasonable since segments close to the observer are more precisely reconstructed by the stereo system than distant ones.
- There is a better agreement in the lateral coordinates of the segments than in the range, because the range component is usually much more uncertain than the other components.
- Those two remarks justify the use of the weighted least-squares property of the Kalman filtering approach.

## 9.2 Rock Scene

As pointed out earlier, our program is developed in the context of visual navigation of a mobile robot in an indoor scene. We expect to be able to describe most of the objects in such an environment by line segments. In this subsection, we describe an example to show that our algorithm works in a cluttered scene containing rocks. Figure 10 shows two images of such a rock scene taken by the first camera of the stereo rig at two instants.

Two 3D frames are reconstructed by our trinocular stereo system which are displayed in Figures 11 and 12. We have obtained 211 3D line segments in the first frame and 208 in the second. Two remarks can be made: the first is that the segments reconstructed are very noisy and even spurious (for example, some are under the ground, as can be observed in the front views); the second is that they are very small. As we can observe, there is a rather big difference between the two frames (about 11 degrees of rotation and 34 centimeters of translation).

In our program, a parameter  $l$ , ranging from  $-5$  to  $5$ , is used to control the thresholds in the rigidity constraints. A change of one for  $l$  corresponds to a change of  $0.2$  for the thresholds. For example, the threshold for the dot-product constraint  $\kappa_c = 1.32 + 0.2l$ . The parameter  $l$  is set to zero in the program, which corresponds to the thresholds indicated in Section 5. When  $l$  decreases, the constraints are imposed more strictly during the hypothesis generation process. When  $l$  increases, the constraints are imposed less strictly. For indoor scenes, we do not need to change  $l$ , *i.e.*, the thresholds are image-independent (they are certainly stereo-system-dependent). However, as the 3D frames reconstructed from the rock scene are very noisy, the motion program generates many false hypotheses although the final result is good. If we set  $l$  to  $-3$ , *i.e.*, we impose more strict rigidity constraints, we obtain five hypotheses. All these hypotheses are propagated to the whole frame to match more segments and to update the motion estimate. In the end, 4 hypotheses give the correct estimate of the displacement.

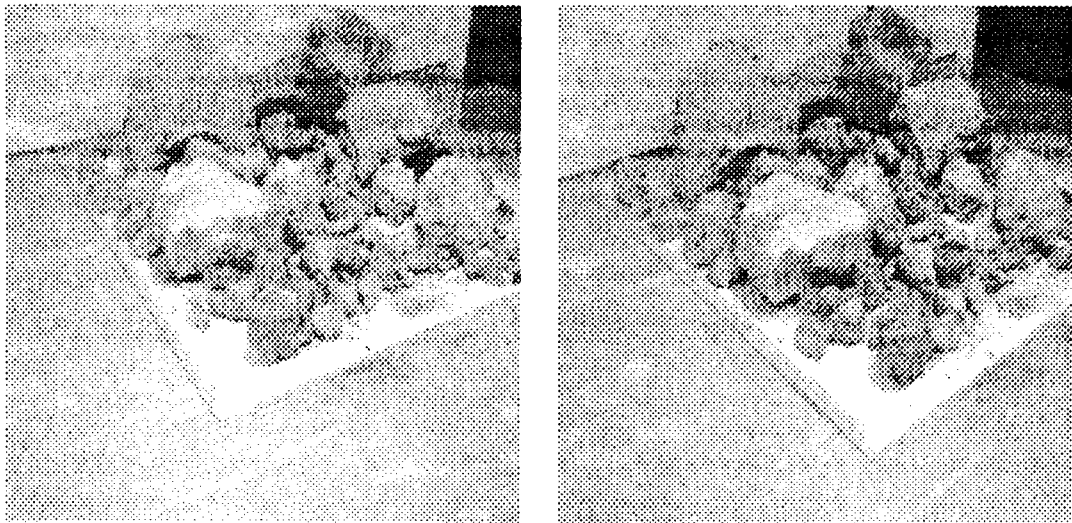


**Fig. 10:** Two images of a rock scene taken by the first camera

93 matches are recovered. To determine how good this estimate is, we apply the computed estimate to the first frame and superimpose the transformed one on the second, which is displayed in Figure 13. We can find that the motion estimate is still very good even for such complicated scene. The displacement of the robot is shown by the shift of the two triangles in the top view of the superposition. The fifth hypothesis gives a suboptimal solution (21 matches are found by this hypothesis). The whole process takes about 50 seconds on a SUN 4 workstation : 40 seconds in the hypothesis generation phase and 10 seconds in the verification phase.

## 10 Application to the Estimation of Multiple Object Displacements

Usually, in a static environment (indoor scene, for example), the observer moves and at the same time there are other moving objects, or the observer is fixed but there exist more than one moving objects (surveillance application, for example). We call this the **multiple object displacement** problem.

The algorithm described above is directly applicable to analyze the multiple object displacement problem. In the hypothesis generation phase, the algorithm tries to find all pairs of pairings of segments between two frames which satisfy the rigidity constraints. Each such pair is an hypothesis of potential displacement between two frames. If two segments in a hypothesis are from a single object, the hypothesis will give the displacement of that object. If an object is made of more than two segments and two of them are precisely reconstructed by the stereo system, then at least one hypothesis among all generated by the algorithm belongs to the object. "Precisely" is, of course, related to the thresholds in the rigidity constraints.

We first apply the algorithm of hypothesis generation to the two observed frames. In order not to miss any potential displacements between them, one modification should be made. Remember that in order to speed up the generation process, we choose only the  $m/q$  ( $q = 2$  or  $3$ )

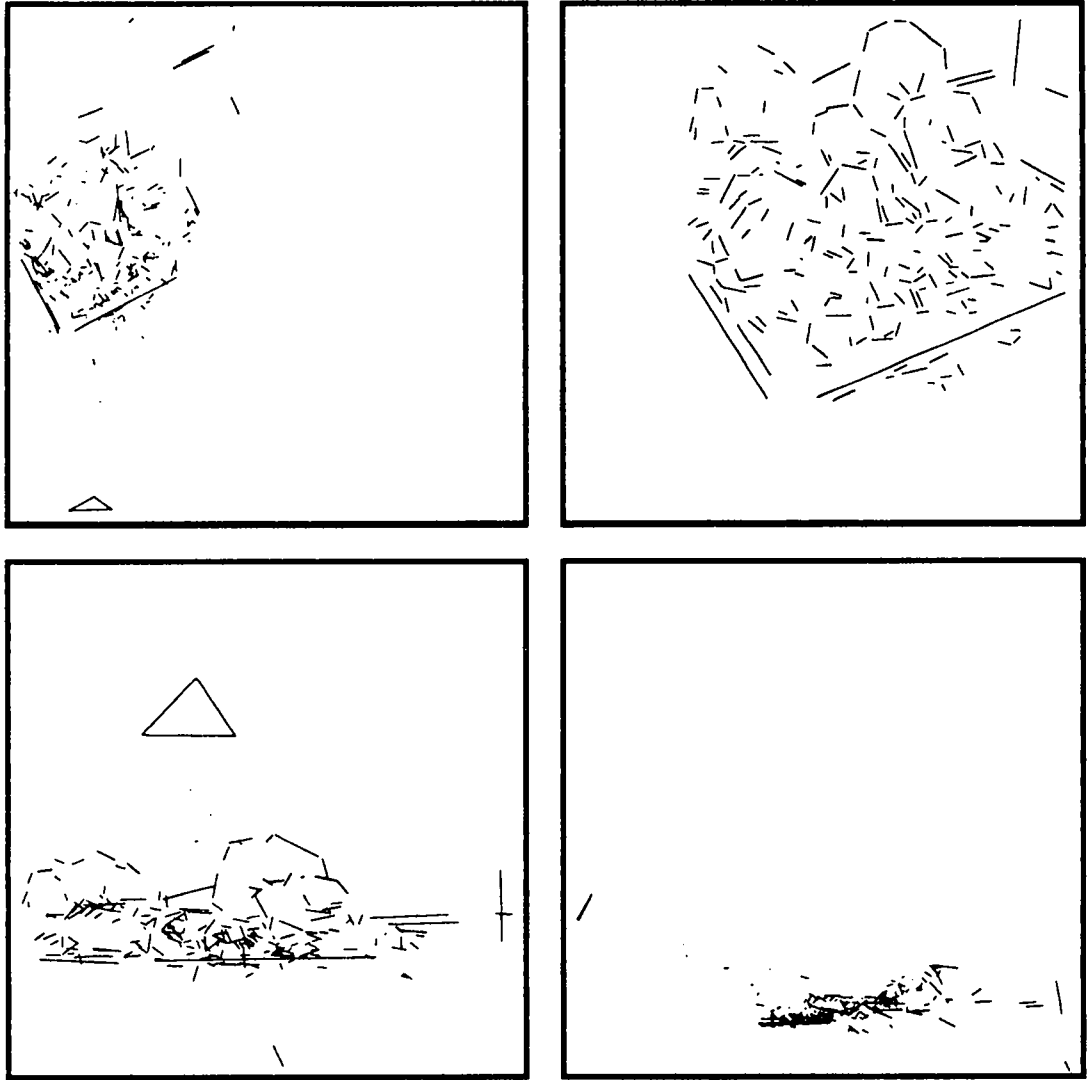


Fig. 11: Different views of stereo frame 1 (uniform scale)



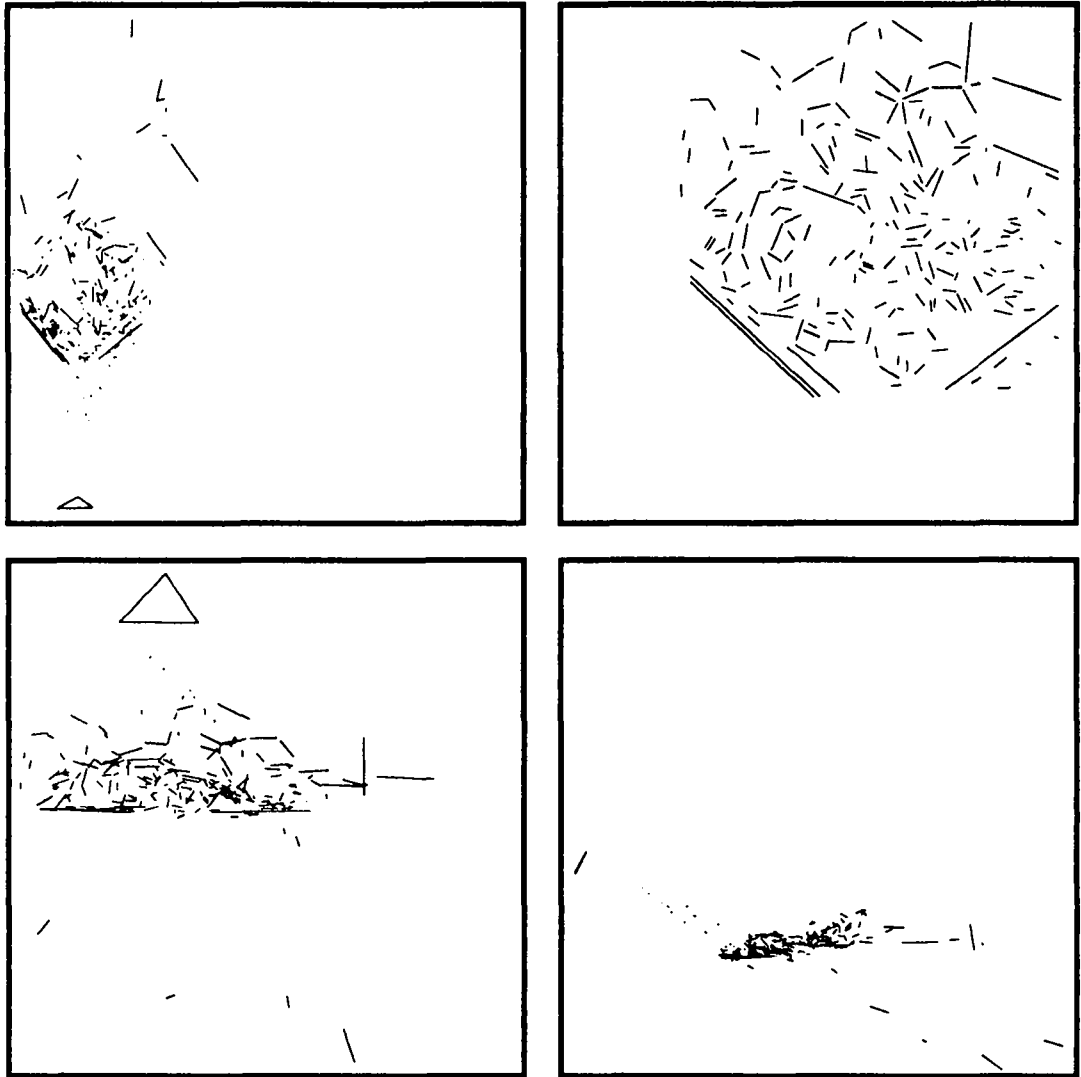
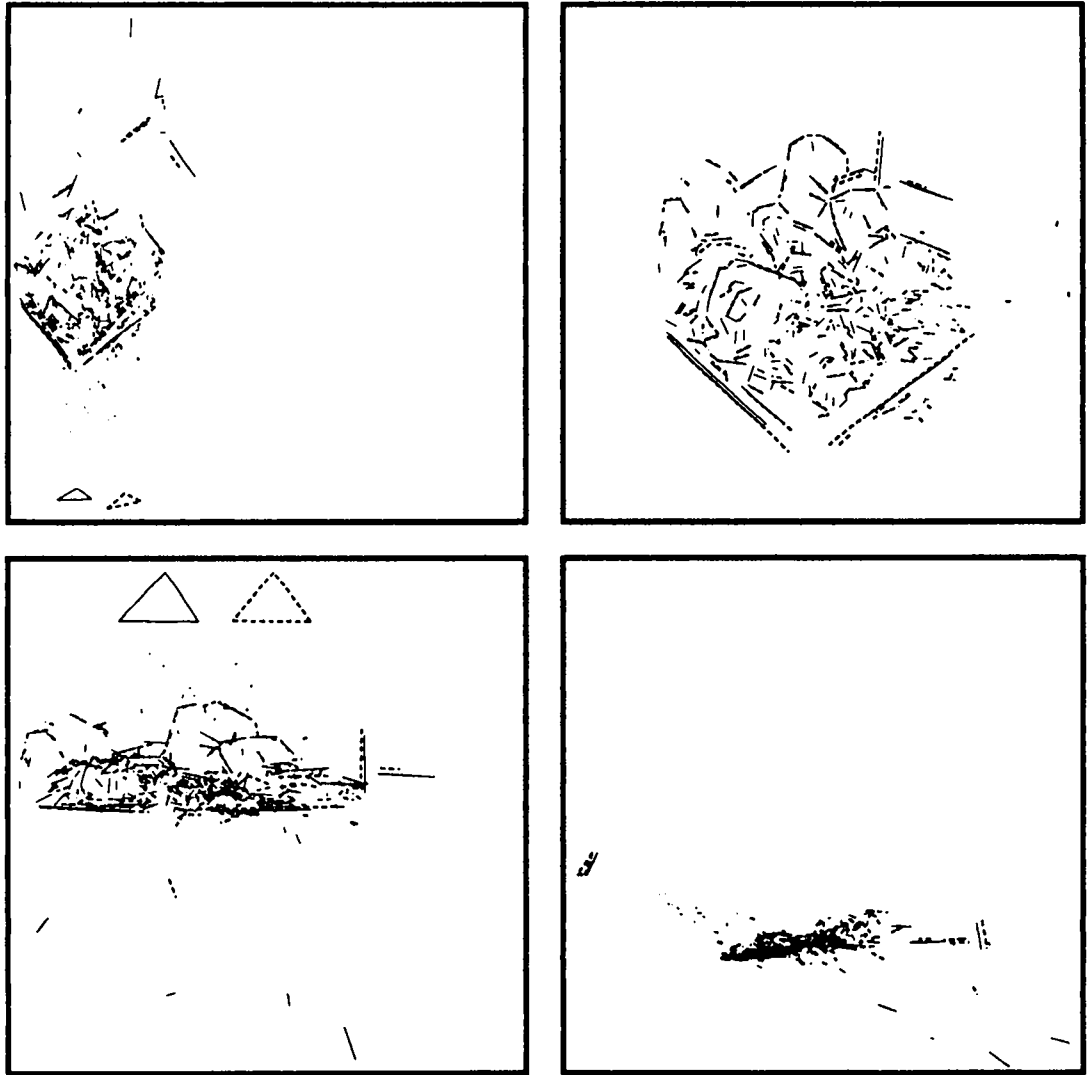


Fig. 12: Different views of stereo frame 2 (uniform scale)



**Fig. 13:** Superposition of the transformed segments of Frame 1 (in dashed lines) and those of Frame 2 (in solid lines) (non-uniform scale)

longest segments in the first frame. It is very likely that for a small object, none of its segments is among the  $m/q$  longest, thus the displacement of such object may not be detected. In order to avoid this, we use all segments in the first frame, *i.e.*, choose  $q = 1$ . Once the hypotheses are generated, we apply the algorithm of hypothesis verification to each of them to update the displacement estimate and to find segment correspondences. We then use the criterion described in Equation 38 to sort those hypotheses. The best one is chosen as the displacement of Object 1 and the corresponding segments in the two frames are labeled as belonging to that object. For each of the other hypotheses, if they are not compatible with any previous one, we retain it as representing a new displacement. In the end, all displacements are recovered and the scene is segmented into objects.

Two methods can be used to test the compatibility of two hypotheses. The first one is to compute the similarity of the corresponding displacement estimates. If the first hypothesis yields a displacement estimate  $\mathbf{s}_1$  with its covariance matrix  $\Lambda_1$ , and the second one yields a displacement estimate  $\mathbf{s}_2$  with its covariance matrix  $\Lambda_2$ , then the Mahalanobis distance between them can be computed as

$$d_s = (\mathbf{s}_1 - \mathbf{s}_2)^T (\Lambda_1 + \Lambda_2)^{-1} (\mathbf{s}_1 - \mathbf{s}_2).$$

The distance  $d_s$  follows a  $\chi^2$  distribution with 6 degrees of freedom. We can choose  $\kappa_s = 12.6$  for a probability of 95%. If the distance between two hypotheses  $d_s \leq \kappa_s$ , they are considered compatible. Another approach is to look at the segment correspondences recovered by the hypotheses. For example, if half of the correspondences recovered by a hypothesis are among those recovered by another hypothesis, then the two hypotheses are considered to be compatible.

In [60], we have described an example of multiple object displacements using synthetic data. There, we discussed also the influence of the egomotion (the displacement of the robot) on the observed object displacements. The example below shows an experiment with a real scene with a real moving object. Figure 14 shows two successive images observed by the first camera of the trinocular stereo rig. Notice that the moving object in the scene is the box in the foreground. It moves from right to left and towards the stereo rig which moves away from the observer. Figures 15 and 16 display the reconstructed 3D scenes in the two positions. Figure 17 shows the overlay of the two 3D frames and the difference between them. There are 168 segments in Frame 1 and 172 segments in Frame 2.

Considering that the static environment contains much more segments than the moving object, we first recover only the egomotion of the stereo rig. Only half of the longest segments in Frame 1 are used in the hypothesis generation process. 16 hypotheses are generated and all of them are evaluated. 8 hypotheses give the estimation of the correct egomotion. Figure 18 shows the estimated egomotion. The shift of the triangle indicates the displacement of the stereo rig. We remark that the two frames are well superimposed, except for the box. From the top view in Figure 18, we easily observe the displacement of the box as indicated by arrows. In fact, five among the 16 hypotheses give the estimation of its displacement, but we do not intend to recover it at this stage, because it may be deteriorated by some occasional bad alignment of segments belonging to the static environment [61].

There remain some unmatched segments. We apply the estimated egomotion to the first frame, and remove the matched segments in the two frames. We thus obtain two 3D frames containing only the segments of the moving object (and several unmatched segments of the environment): the effect of the egomotion has been eliminated. The superposition of two

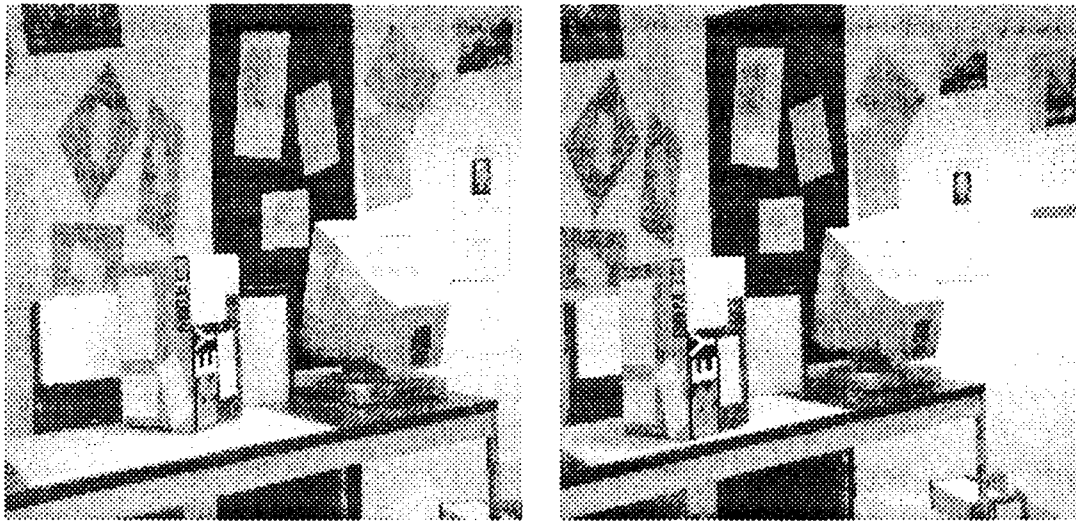


**Fig. 14:** Images of the first camera of the trinocular stereo rig: the left one is in the first position and the right one is in the second position

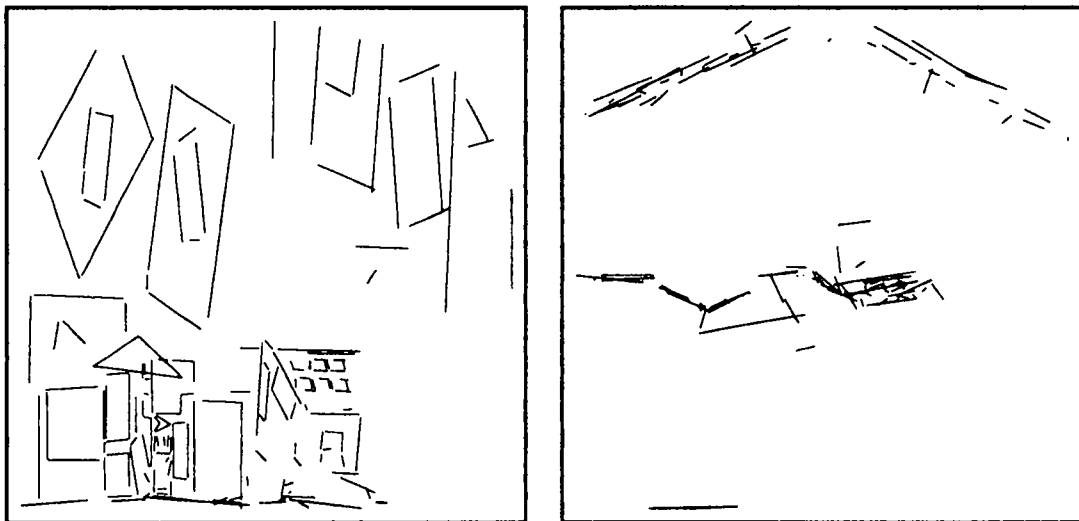


**Fig. 15:** The front and top views of the reconstructed 3D frame in the first position

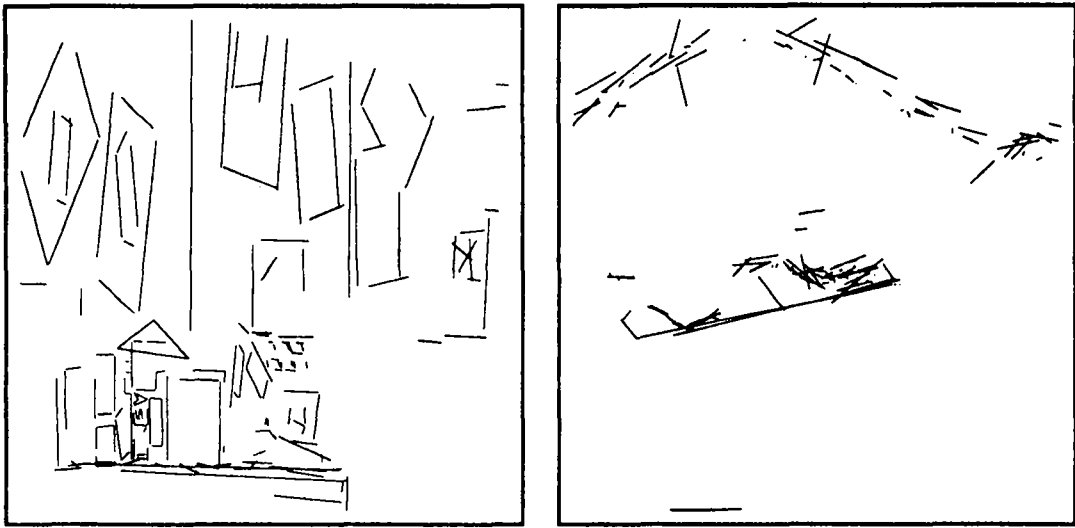


Fig. 16: The front and top views of the reconstructed 3D frame in the second position

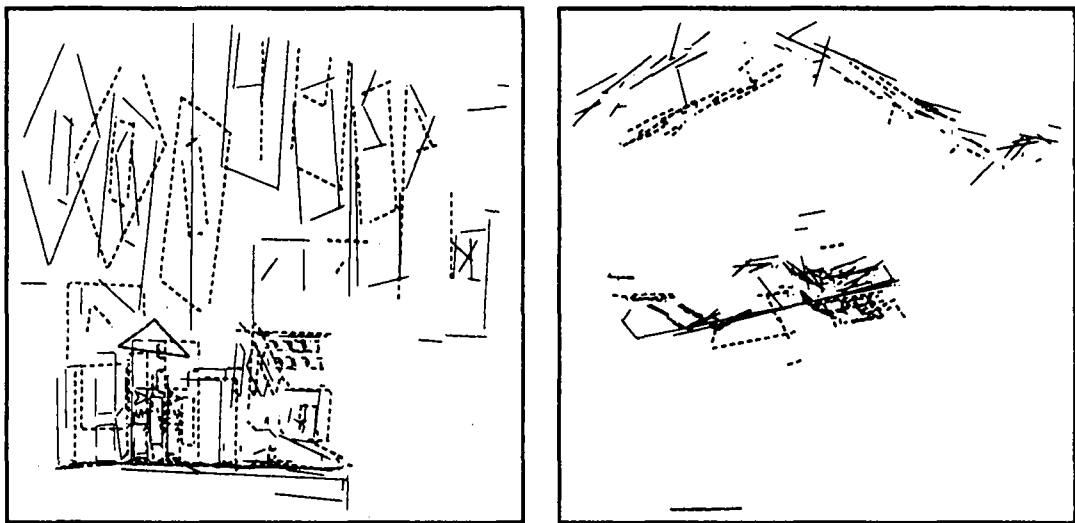


Fig. 17: Superposition of the two original frames

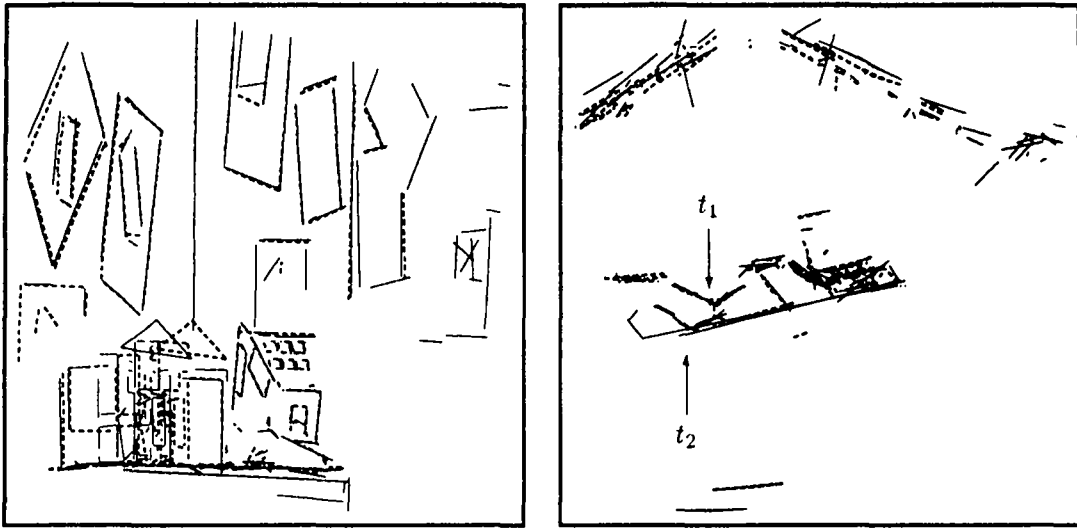


Fig. 18: Superposition of the segments of Frame 1 after applying the estimated egomotion and those of Frame 2

such frames is displayed in Figure 19. This figure clearly shows the movement of the box, as indicated by arrows.

We then apply the same process as before on these two sets of segments. All segments are used in the hypothesis generation phase. 6 hypotheses are generated and they are all evaluated. All yield the correct displacement of the box. The result is shown in Figure 20. We can remark that the segments of the box superimpose very well.

## 11 Conclusion

We have developed an approach based on the *hypothesize-and-verify* paradigm for registering two stereo frames and computing the 3D displacement between them. The rigidity constraints are used to generate hypotheses of feature correspondences between two frames. We have shown that the rigidity constraints we have formulated are complete for 3D line segments and that a unique rigid displacement can be computed from two pairings of segments satisfying those constraints. The uncertainty of measurements has been integrated into the formalism of the rigidity constraints. If two pairings of segments satisfy the rigidity constraint, they are retained as an hypothesis. An initial estimate of the displacement can then be computed for each hypothesis. This initial estimate is propagated to the whole frame in an attempt to match more segments. Each time a new match is obtained, the displacement estimate is updated. Finally, the best hypothesis is retained. This algorithm has been successfully tested with several hundreds of real stereo frames

We have also extended it to determine multiple object displacements. When the robot navigates in an environment in which there exist other moving rigid objects, our algorithm first determines the egomotion and then cancels it before recovering the object displacements.

The proposed algorithm is easily adapted to solve simple object recognition and location problem (see [61] for more details). It has many other interesting applications, such as visually guided navigation [78] and world model building [69].

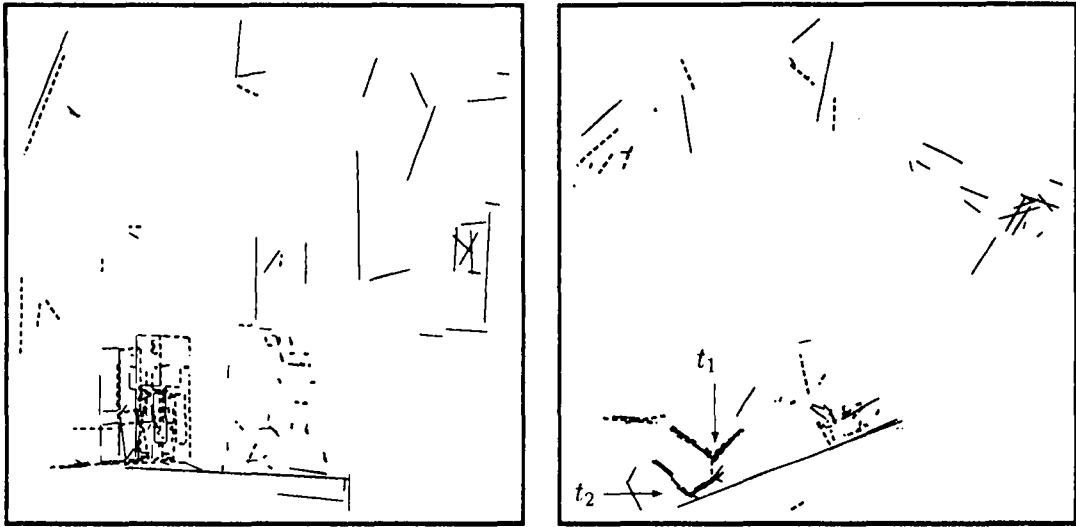


**Fig. 19:** Superposition of the remaining segments of both frames after those matched through the egomotion estimation procedure have been eliminated

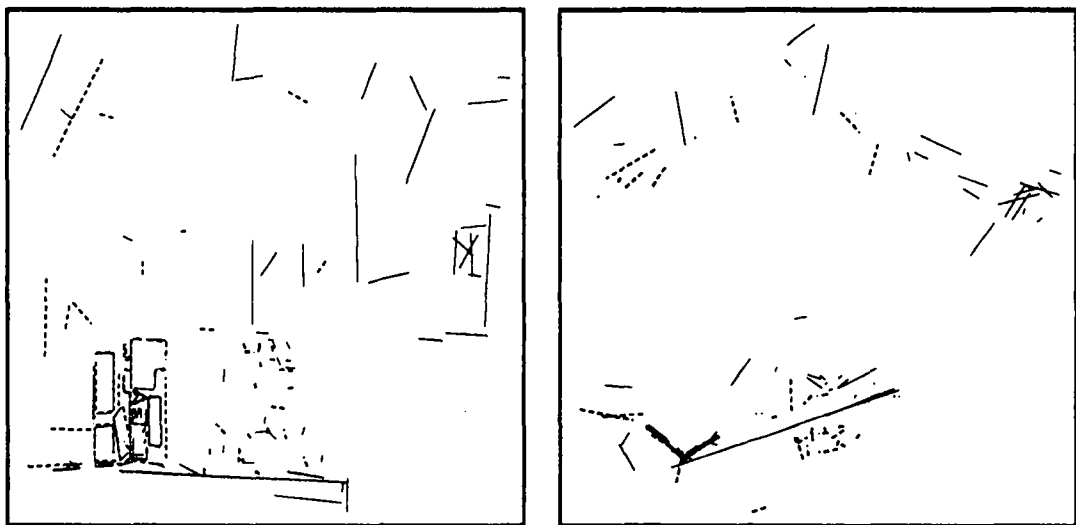


**Fig. 20:** Result of applying the estimated displacement of the box

Although the proposed algorithm has been successfully tested using a large number of scenes, the primitive used (3D line segment) is rather limited. It is usually not sufficient to interpret complex scenes with only line segments. Our current research consists in developing strategies to include other primitives such as points, curves, and surface patches.

### Appendix: Proof of Proposition 3

The proof of Proposition 3 requires the definition of the congruency of two tetrahedra since by linking the endpoints of two non-coplanar line segments, we get a tetrahedron.

**Definition 2** *Two tetrahedra are said to be congruent if and only if the following relations hold:*

1.  $\|\overline{V_i V_j}\| = \|\overline{V'_i V'_j}\|$ , for  $i, j = 1 \dots 4$  and  $i \neq j$ ,
2.  $\langle \overline{V_1 V_2}, \overline{V_3 V_4}, \overline{V_3 V_1} \rangle = \langle \overline{V'_1 V'_2}, \overline{V'_3 V'_4}, \overline{V'_3 V'_1} \rangle$ ,

where  $\{V_i, (i = 1 \dots 4)\}$  are the vertices of the first tetrahedron and  $\{V'_i, (i = 1 \dots 4)\}$  those of the second.  $\diamond$

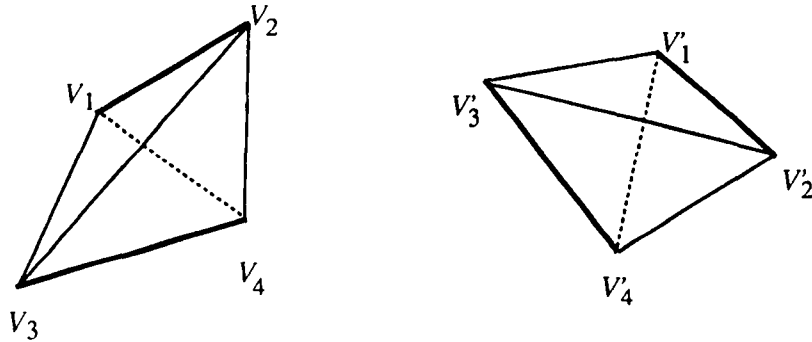


**Fig. 21:** Congruency of two tetrahedra

Figure 21 shows two congruent tetrahedra. The first condition of Definition 2 guarantees that the two tetrahedra are *isometric*, i.e., two congruent tetrahedra equal length corresponding edges. This condition, however, is not sufficient, because it cannot disambiguate two tetrahedra corresponding to each other through a *rotation* from those corresponding to each other through a *reflection* about the coordinate system. Figure 22 shows an example of reflection of two tetrahedra. In this figure, the two tetrahedra satisfy the first condition of Definition 2, but they are not congruent. For example, if we bring  $V_1, V_2, V_3$  into correspondence with  $V'_1, V'_2, V'_3$  and put them together, we see that  $V_4$  and  $V'_4$  are located on the different sides of the plane containing  $V_1, V_2$  and  $V_3$ . If we compute the transformation for these two tetrahedra, we get an orthogonal transformation whose determinant is  $-1$ . The second condition of Definition 2 is there to avoid this case.

**Proof of Proposition 3:** Three cases exist depending upon the configuration of the two line segments.



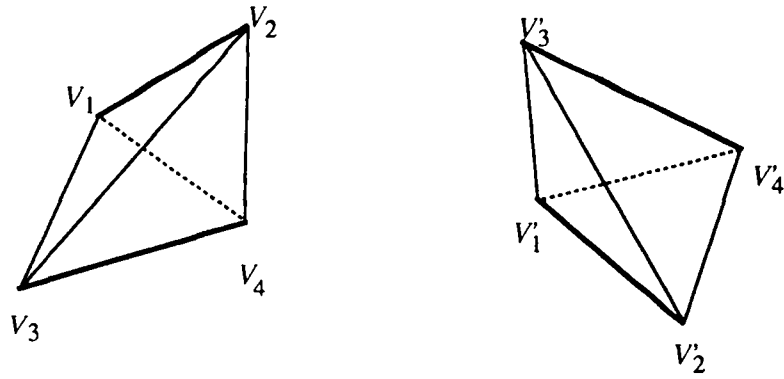


Fig. 22: Reflection of two tetrahedra

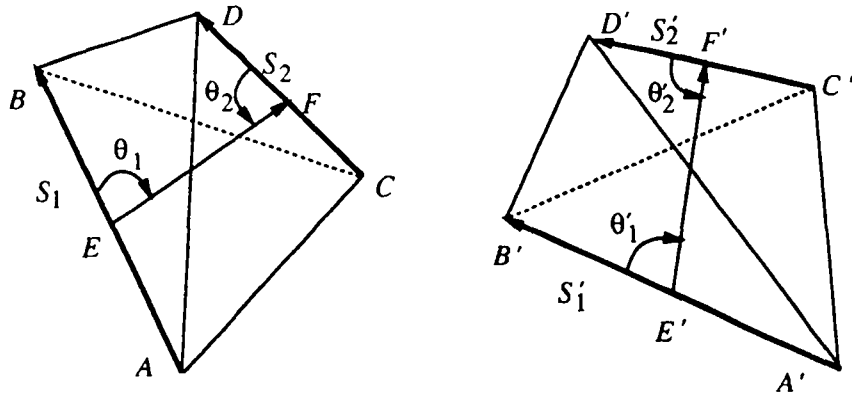


Fig. 23: Completeness of the rigidity constraints: non-coplanar case

**Case 1: The two line segments are not coplanar** In this case, the two line segments form a tetrahedron by linking their endpoints (see Figure 23). We only need to show that if two pairings of segments satisfy all the constraints described in Proposition 2, then their resulting tetrahedra are congruent. The following equations relate the symbols for points in Figure 23 to the parameters of segments:

$$\begin{aligned}
 A &= \mathbf{b}_1, & B &= \mathbf{e}_1, & C &= \mathbf{b}_2, & D &= \mathbf{e}_2, & E &= \mathbf{m}_1, & F &= \mathbf{m}_2, \\
 A' &= \mathbf{b}'_1, & B' &= \mathbf{e}'_1, & C' &= \mathbf{b}'_2, & D' &= \mathbf{e}'_2, & E' &= \mathbf{m}'_1, & F' &= \mathbf{m}'_2.
 \end{aligned} \tag{55}$$

What we should verify is then (from Definition 2) <sup>†</sup>

$$AB = A'B'; \tag{56}$$

$$CD = C'D'; \tag{57}$$

---

<sup>†</sup>In the proof,  $AB$  and  $\|\overline{AB}\|$  are synonymous.

$$AC = A'C'; \quad (58)$$

$$AD = A'D'; \quad (59)$$

$$BC = B'C'; \quad (60)$$

$$BD = B'D'; \quad (61)$$

$$\langle \overrightarrow{AB}, \overrightarrow{CD}, \overrightarrow{AC} \rangle = \langle \overrightarrow{A'B'}, \overrightarrow{C'D'}, \overrightarrow{A'C'} \rangle. \quad (62)$$

From the length constraints given in Proposition 2, Equations 56 and 57 are satisfied. Now we examine Equation 58. Since

$$\overrightarrow{AC} = \mathbf{b}_2 - \mathbf{b}_1 = (\mathbf{b}_2 - \mathbf{m}_2) + (\mathbf{m}_2 - \mathbf{m}_1) + (\mathbf{m}_1 - \mathbf{b}_1) = -l_2 \mathbf{u}_2/2 + \mathbf{v}_{12} + l_1 \mathbf{u}_1/2,$$

we have

$$\begin{aligned} AC^2 &= \overrightarrow{AC} \cdot \overrightarrow{AC} = (-l_2 \mathbf{u}_2/2 + \mathbf{v}_{12} + l_1 \mathbf{u}_1/2) \cdot (-l_2 \mathbf{u}_2/2 + \mathbf{v}_{12} + l_1 \mathbf{u}_1/2) \\ &= (l_1^2 + l_2^2)/4 + (\mathbf{v}_{12} \cdot \mathbf{v}_{12}) - l_1 l_2 (\mathbf{u}_1 \cdot \mathbf{u}_2)/2 + l_1 (\mathbf{u}_1 \cdot \mathbf{v}_{12}) - l_2 (\mathbf{u}_2 \cdot \mathbf{v}_{12}). \end{aligned}$$

Similarly, we have

$$A'C'^2 = (l_1'^2 + l_2'^2)/4 + (\mathbf{v}'_{12} \cdot \mathbf{v}'_{12}) - l_1' l_2' (\mathbf{u}'_1 \cdot \mathbf{u}'_2)/2 + l_1' (\mathbf{u}'_1 \cdot \mathbf{v}'_{12}) - l_2' (\mathbf{u}'_2 \cdot \mathbf{v}'_{12}).$$

From the length, distance and angular constraints given in Proposition 2, we get

$$AC^2 = A'C'^2.$$

Equation 58 is then verified. In the same manner, we can show that Equations 59 to 61 are also true.

It remains to verify Equation 62. In fact, we have

$$\begin{aligned} \langle \overrightarrow{AB}, \overrightarrow{CD}, \overrightarrow{AC} \rangle &= \overrightarrow{AB} \cdot (\overrightarrow{CD} \wedge \overrightarrow{AC}) = l_1 \mathbf{u}_1 \cdot (l_2 \mathbf{u}_2 \wedge (-l_2 \mathbf{u}_2/2 + \mathbf{v}_{12} + l_1 \mathbf{u}_1/2)) \\ &= l_1 l_2 \mathbf{u}_1 \cdot (\mathbf{u}_2 \wedge \mathbf{v}_{12}) = l_1 l_2 \|\mathbf{v}_{12}\| \langle \mathbf{u}_1, \mathbf{u}_2, \hat{\mathbf{v}}_{12} \rangle, \end{aligned}$$

and

$$\langle \overrightarrow{A'B'}, \overrightarrow{C'D'}, \overrightarrow{A'C'} \rangle = l_1' l_2' \|\mathbf{v}'_{12}\| \langle \mathbf{u}'_1, \mathbf{u}'_2, \hat{\mathbf{v}}'_{12} \rangle.$$

From the length, distance and triple product constraints given in Proposition 2, we see that Equation 62 is true.

**Case 2: Two line segments are coplanar and not collinear** In this case, the tetrahedron degenerates to a quadrilateral (see Figure 24). The necessary-sufficient conditions of congruency of two quadrilaterals are

$$AB = A'B', CD = C'D', AC = A'C', BD = B'D', \text{ and } \overrightarrow{AB} \cdot \overrightarrow{AC} = \overrightarrow{A'B'} \cdot \overrightarrow{A'C'}.$$

One can easily verify that these conditions are satisfied given the rigidity constraints in Proposition 2.

**Case 3: Two line segments are collinear** In this special case, the local shape is determined by the lengths of two segments, the separation between them and their relative position. We can show that the rigidity constraints guarantee the preservation of the local shape. Since it does not allow us to recover fully the rigid motion, this special configuration is not considered furthermore.

This ends the proof. ■

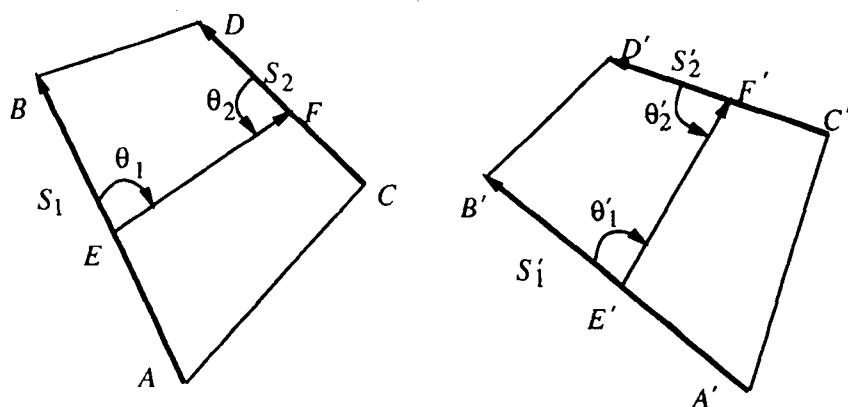


Fig. 24: Completeness of the rigidity constraints: coplanar case

## Acknowledgement

The authors would like to thank Nicholas Ayache for his contribution to the work presented in this paper.

## References

- [1] T. Huang. "Motion analysis," in *AI Encyclopedia*, pp. 620-632, New York: John Wiley, 1986.
- [2] H. Nagel. "Image sequences - ten (octal) years- from phenomenology towards a theoretical foundation." in *Proceedings 8th ICPR*, (Paris, France), pp. 1174-1185, IEEE, October 1986.
- [3] J. Aggarwal and N. Nandhakumar, "On the computation of motion from sequences of images --- a review." *Proceedings of the IEEE*, vol. 76, pp. 917-935, August 1988.
- [4] S. Barnard and M. Fishler, "Computational stereo," *ACM Computing Surveys*, vol. 14, no. 4, pp. 553-572, 1982.
- [5] W. Grimson, "Computational experiments with a feature based stereo algorithm," *IEEE Transactions on Pattern Analysis and Machine Intelligence*, vol. 7, no. 1, pp. 17-34, 1985.
- [6] S. Pollard, J. Mayhew, and J. Frisby, "PMF: a stereo correspondence algorithm using a disparity gradient limit," *Perception*, vol. 14, pp. 449-470, 1985.
- [7] N. Ayache and B. Faverjon, "A fast stereo vision matcher based on prediction and recursive verification of hypotheses," in *Proceedings of Third Workshop on Computer Vision: Representation and Control*, pp. 27-37, IEEE, October 1985. Shorter version in CVPR '85, San Francisco. 1985.

- [8] N. Ayache and F. Lustman, "Fast and reliable passive trinocular stereovision," in *Proc. First International Conference on Computer Vision*, (London, UK), pp. 422-427, IEEE, June 1987.
- [9] O. Faugeras *et al.*, "Toward a flexible vision system," in *Robot Vision*, (A. Pugh, ed.), ch. 3, pp. 129-142, UK: IFS, 1983.
- [10] B. Horn and B. Schunk, "Determining optical flow," *Artificial Intelligence*, vol. 20, pp. 199-228, 1981.
- [11] B. Horn, *Robot Vision*. MIT Press and McGraw-Hill Book Company, 1986.
- [12] H. Nagel, "Displacement vectors derived from second-order intensity variations in image sequences," *Computer Vision, Graphics, and Image Processing*, vol. 21, pp. 85-117, 1983.
- [13] E. Hildreth. *The Measurement of Visual Motion*. MIT Press, Cambridge, 1983.
- [14] A. Bruss and B. Horn, "Passive navigation," *Computer Vision, Graphics, and Image Processing*, vol. 21, pp. 3-20, January 1983.
- [15] G. Adiv, "Inherent ambiguities in recovering 3D motion and structure from a noisy flow field," in *Proc. IEEE Conference on Computer Vision and Pattern Recognition*, pp. 70-77, June 1985. San Francisco, CA.
- [16] S. Maybank, *A Theoretical Study of Optical Flow*. PhD thesis, Birkbeck College, University of London., London, UK, 1987.
- [17] A. Waxman and J. Duncan, "Binocular image flows: steps toward stereo-motion fusion," *IEEE Transactions on Pattern Analysis and Machine Intelligence*, vol. PAMI-8, pp. 715-729, November 1986.
- [18] A. Waxman and S. Sinha, "Dynamic stereo: passive ranging to moving objects from relative image flows," *IEEE Transactions on Pattern Analysis and Machine Intelligence*, vol. PAMI-8, pp. 406-412, July 1986.
- [19] J. Heel, "Dynamic motion vision," in *Proceedings of the DARPA Image Understanding Workshop*, (Palo Alto, CA). May 1989.
- [20] S. Ullman. *The Interpretation of Visual Motion*. MIT Press, Cambridge, 1979.
- [21] R. Tsai and T. Huang, "Estimating 3-D motion parameters of a rigid planar patch, i," *IEEE Transactions on Acoustic, Speech and Signal Processing*, vol. ASSP-29, pp. 1147-1152, December 1981.
- [22] T. Huang and R. Tsai, "Image sequence analysis: motion estimation," in *Image Sequence Processing and Dynamic Scene Analysis*, (T. Huang, ed.), New York: NY: Springer-Verlag, 1981.
- [23] H. Longuet-Higgins, "A computer algorithm for reconstructing a scene from two projections." *Nature*, vol. 293, pp. 133-135. 1981.
- [24] B. Yen and T. Huang, "Determining 3-D motion/structure of a rigid body over 3 frames using straight line correspondences," in *Proc. IEEE Conference on Computer Vision and Pattern Recognition*, (Washington, DC). pp. 267-272, IEEE, June 19-23 1983.
- [25] R. Tsai and T. Huang, "Uniqueness and estimation of three-dimensional motion parameters of rigid objects with curved surface," *IEEE Transactions on Pattern Analysis and Machine Intelligence*, vol. PAMI-6, pp. 13-26, Jan. 1984.

- [26] X. Zhuang and R. Haralick, "Two view motion analysis," in *Proceedings CVPR '85, San Francisco, California*, pp. 686-690, June 1985.
- [27] Y. Liu and T. Huang, "Estimation of rigid body motion using straight line correspondences," in *Proceedings Workshop on Motion: Representation and Analysis, Charleston, South Carolina, USA*, pp. 47-51, IEEE, May 1986.
- [28] A. Mitiche, S. Seida, and J. Aggarwal, "Line based computation of structure and motion using angular invariance," in *Proceedings Workshop on Motion: Representation and Analysis, (Charleston, South Carolina, USA)*, pp. 175-180, IEEE, May 1986.
- [29] O. Faugeras, F. Lustman, and G. Toscani, "Motion and structure from motion from point and line matches," in *Proc. First International Conference on Computer Vision*, pp. 25-34, 1987.
- [30] J. Aggarwal and Y. Wang, "Analysis of a sequence of images using point and line correspondences," in *Proc. International Conference on Robotics and Automation, (Raleigh, NC)*, pp. 1275-1280, IEEE, March 31-April 3 1987.
- [31] O. Faugeras and S. Maybank, "Motion from point matches: multiplicity of solutions," *The International Journal of Computer Vision*, vol. 4, pp. 225-246, June 1990.
- [32] T. Broida and R. Chellappa, "Kinematics and structure of a rigid object from a sequence of noisy images: a batch approach," in *Proc. IEEE Conf. Computer Vision and Pattern Recognition, (Miami Beach, FL)*, pp. 176-182, IEEE, June 1986.
- [33] T. Broida and R. Chellappa, "Experiments and uniqueness results on object structure and kinematics from a sequences of monocular images," in *Proc. IEEE Workshop on Visual Motion, (Irvine, CA)*, pp. 21-30, IEEE, March 1989.
- [34] J. Weng, T. Huang, and N. Ahuja, "3-D motion estimation, understanding, and prediction from noisy image sequences," *IEEE Transactions on Pattern Analysis and Machine Intelligence*, vol. PAMI-9, no. 3, pp. 370-389, 1987.
- [35] G. Young and R. Chellappa, "3-D motion estimation using a sequence of noisy stereo images: models, estimation, and uniqueness results," *IEEE Transactions on Pattern Analysis and Machine Intelligence*, vol. 12, pp. 735-759, August 1990.
- [36] Z. Zhang and O. Faugeras, "Tracking and grouping 3D line segments," in *Proc. 3rd International Conference on Computer Vision, (Osaka, Japan)*, pp. 577-580, IEEE, December 1990.
- [37] H. Shariat and K. Price, "Motion estimation with more than two frames," *IEEE Transactions on Pattern Analysis and Machine Intelligence*, vol. 12, pp. 417-434, May 1990.
- [38] T. Broida, S. Chandrashekhar, and R. Chellappa, "Recursive 3-D motion estimation from a monocular image sequence," *IEEE Trans. on Aerospace and Electronic Systems*, vol. 26, pp. 639-656, July 1990.
- [39] S. Pollard, J. Porrill, J. Mayhew, and J. Frisby, "Matching geometrical descriptions in three-space," *Image and Vision Computing*, vol. 5, pp. 73-78, may 1987.
- [40] R. Bolles and R. Cain, "Recognizing and locating partially visible objects, the local-feature-focus method," *International Journal of Robotics Research*, vol. 1, no. 3, pp. 57-82, 1982.

- [41] P. Horaud and R. Bolles, "3DPO's strategy for matching three-dimensional objects in range data," in *Proc. of the International Conference on Robotics and Automation*, (Atlanta, Ga.), pp. 78-85, IEEE, March 13-15 1984.
- [42] W. Grimson and T. Lozano-Perez, "Model-based recognition and localization from sparse range or tactile data," *International Journal on Robotics Research*, vol. 5, pp. 3-34, Fall 1984.
- [43] H. Chen and T. Huang, "Maximal matching of 3-D points for multiple-object motion estimation," *Pattern Recognition*, vol. 21, no. 2, pp. 75-90, 1988.
- [44] H. Chen and T. Huang, "An algorithm for matching 3-D line segments with application to multiple object motion estimation," in *Proc. of the IEEE Computer Society, Workshop on Computer Vision*, pp. 151-156, 1987. November 30-December 2.
- [45] Y. Kim and J. Aggarwal, "Determining object motion in a sequence of stereo images," *IEEE Journal of Robotics and Automation*, vol. 3, pp. 599-614, December 1987.
- [46] S. Blostein and T. Huang, "Estimation 3-D motion from range data," in *The First Conference on Artificial Intelligence Applications*, pp. 246-250, December 5-7 1984.
- [47] T. Huang and S. Blostein, "Robust algorithms for motion estimation based on two sequential stereo image pairs," in *Proc. Conf. on Computer Vision and Pattern Recognition*, (San Francisco), pp. 518-523, IEEE, 1985.
- [48] O. Faugeras and M. Hebert, "The representation, recognition, and locating of 3D shapes from range data," *The International Journal of Robotics Research*, vol. 5, no. 3, pp. 27-52, 1986.
- [49] O. Faugeras, N. Ayache, and B. Faverjon, "Building visual maps by combining noisy stereo measurements," in *Proceedings of the Conference on Robotics and automation*, IEEE, April 1986.
- [50] N. Ayache and O. Faugeras, "Building, registering and fusing noisy visual maps," in *Proceedings ICCV '87, London*, pp. 73-82, IEEE, June 1987.
- [51] Z. Lin, H. Lee, and T. Huang, "Finding 3-D point correspondence in motion estimation," in *Proc. Fifth International Conference on Pattern Recognition*, 1986.
- [52] W. Grimson and T. Lozano-Perez, "Localizing overlapping parts by searching the interpretation tree," *IEEE Transactions on Pattern Analysis and Machine Intelligence*, vol. 7, no. 4, pp. 469-482, 1987.
- [53] R. Bolle and D. Cooper, "On optimally combining pieces of information with application to estimating 3-D complex-object position from range data," *IEEE Transactions on Pattern Analysis and Machine Intelligence*, vol. PAMI-8, no. 5, pp. 619-638, 1986.
- [54] G. Stockman, "Object recognition and localization via pose clustering," *Computer Vision, Graphics, and Image Processing*, no. 40, pp. 361-387, 1987.
- [55] D. Thompson and J. Mundy, "Three-dimensional model matching from an unconstrained viewpoint," in *Proc. International Conference on Robotics and Automation*, (Raleigh, NC, USA), pp. 208-220, 1987.
- [56] N. Ayache and O. Faugeras, "Hyper: a new approach for the recognition and positioning of two-dimensional objects," *IEEE Transactions on PAMI*, vol. 8, pp. 44-54, January 1986.

- [57] D. Lowe, *Perceptual Organization and Visual Recognition*. Kluwer Academic Publishers, 1985.
- [58] D. Lowe, "The viewpoint consistency constraint," *International Journal of Computer Vision*, no. 1, pp. 57-72, 1987.
- [59] O. Faugeras, N. Ayache, and Z. Zhang, "A preliminary investigation of the problem of determining ego- and object motions from stereo," in *Proc. 9th International Conference on Pattern Recognition*, (Rome, Italy), pp. 242-246, 1988.
- [60] Z. Zhang, O. Faugeras, and N. Ayache, "Analysis of a sequence of stereo scenes containing multiple moving objects using rigidity constraints," in *Proc. Second International Conference on Computer Vision*, (Tampa, Florida), pp. 177-186, IEEE, December 1988.
- [61] Z. Zhang, *Motion Analysis from a Sequence of Stereo Frames and its Applications*. PhD thesis, University of Paris-Sud, Orsay, Paris, France, 1990. in English.
- [62] H. Durrant-Whyte, "Uncertain geometry in robotics," *IEEE Journal of Robotics and Automation*, vol. 4, pp. 23-31, February 1988.
- [63] N. Ayache and O. Faugeras, "Maintaining representations of the environment of a mobile robot," in *International Symposium on Robotics Research*, MIT Press, August 1987. Santa-Cruz, California.
- [64] S. Blostein and T. Huang, "Error analysis in stereo determination of a 3-D point position," *IEEE Transactions on Pattern Analysis and Machine Intelligence*, vol. PAMI-9, pp. 752-765, November 1987.
- [65] L. Matthies and S. A. Shafer, "Error modeling in stereo navigation," *IEEE Journal on Robotics and Automation*, vol. RA-3, pp. 239-248, June 1987.
- [66] N. Ayache and O. D. Faugeras, "Maintaining Representations of the Environment of a Mobile Robot," *IEEE transactions on Robotics and Automation*, vol. 5, pp. 804-819, December 1989.
- [67] N. Ayache, *Construction et Fusion de Représentations Visuelles 3D - Applications à la Robotique Mobile*. PhD thesis, University of Paris XI, Paris-Orsay, 1988. Thèse d'Etat.
- [68] K. Roberts, "A new representation for a line," in *Proc. of the 1988 Conference on Computer Vision and Pattern Recognition*, (Ann Arbor, Michigan), pp. 635-640, IEEE, June 5-9 1988.
- [69] Z. Zhang and O. Faugeras, "Building a 3D world model with a mobile robot: 3D line segment representation and integration," in *Proc. 10th International Conference on Pattern Recognition*, (Atlantic City, New Jersey, USA), pp. 38-42, IEEE, June 1990.
- [70] D. Murray and D. Cook, "Using the orientation of fragmentary 3D edge segments for polyhedral object recognition," *International Journal of Computer Vision*, no. 2, pp. 153-169, 1988.
- [71] K. Arun, T. Huang, and S. Blostein, "Least-squares fitting of two 3-D point sets," *IEEE Transactions on Pattern Analysis and Machine Intelligence*, vol. PAMI-9, pp. 698-700, September 1987.
- [72] Z. Zhang and O. Faugeras, "Determining motion from 3D line segments: a comparative study," in *Proc. British Machine Vision Conference 1990*, (University of Oxford), pp. 85-90, 24th - 27th September 1990.

- [73] A. Jazwinsky, *Stochastic Processes and Filtering Theory*. Academic Press, 1970.
- [74] P. Maybeck. *Stochastic Models, Estimation and Control*. Vol. 1, Academic Press, 1979.
- [75] P. Maybeck, *Stochastic Models, Estimation and Control*. Vol. 2, Academic Press, 1982.
- [76] O. Faugeras, "A few steps toward artificial 3D vision," in *Robotics Science*, (M. Brady, ed.), ch. 2, pp. 39-137, MIT Press, 1989.
- [77] O. Rodrigues, "Des lois géométriques qui régissent les déplacements d'un système solide dans l'espace, et de la variation des coordonnées provenant de ces déplacements considérés indépendamment des causes qui peuvent les produire," *Journal de Mathématiques Pures et Appliquées*, vol. 5, pp. 380-440, 1840.
- [78] Z. Zhang and O. Faugeras, "Calibration of a mobile robot with application to visual navigation," in *Proc. IEEE Workshop on Visual Motion*, (Irvine, California), pp. 306-313, IEEE, March 20-22 1989.



**ISSN 0249 - 6399**